Formation and Evolution of Protoplanetary Discs

Appelgren, Johan

2024

Formation and Evolution of Protoplanetary Discs

JOHAN APPELGREN
LUND OBSERVATORY | DEPARTMENT OF PHYSICS | LUND UNIVERSITY

Printed by Media-Tryck, Lund 2024 NORDIC SWAN ECOLABEL 3041 0903

Faculty of Science
Department of Physics
Division of Astrophysics
Lund Observatory

ISBN 978-91-8039-898-5

Formation and Evolution of Protoplanetary Discs

Johan Appelgren

LUND
UNIVERSITY

Thesis for the degree of Doctor of Philosophy

Thesis advisor: Prof. Anders Johansen
Faculty opponent: Dr. Paola Pinilla

To be presented, with the permission of the Faculty of Science of Lund University, for public criticism in the Lundmark lecture hall (Lundmarksalen) at the Astronomy house (Astronomihuset) on Thursday, 14th of March 2024 at 09:00.

Organization LUND UNIVERSITY Division of Astrophysics, Department of Physics, Box 118, SE-221 00, Lund, Sweden	**Document name** DOCTORAL DISSERTATION
	Date of issue 2024-02-19
Author(s) Johan Appelgren	Sponsoring organization

Title and subtitle
Formation and Evolution of Protoplanetary Discs

Abstract

Protoplanetary discs and the protostars they surround are formed from the gravitational collapse of molecular cloud cores. These discs consist primarily of gas, with a small but important dust component. The roughly mm-sized grains that make up the dust component are the building blocks of planets. Over a timescale of up to a few million years, the dust in protoplanetary discs is lost. Some of the dust will be locked up into planetesimals and planets, but the majority of the decrease in the dust mass is likely caused by the radial drift of pebbles.

In this thesis, I have studied the evolution of protoplanetary discs, with a focus on the evolution of the dust disc through the radial drift of pebbles. I developed a numerical model that includes the formation of the disc from a collapsing molecular cloud core, viscous evolution and photoevaporation of the gas disc, as well as the growth and radial drift of the dust disc.

In Papers I and II, we explored the temporal evolution of the dust mass in protoplanetary discs due to radial pebble drift using a population synthesis approach. We found that discs undergoing radial pebble drift can sustain sufficient dust masses for long enough to explain the observed decrease in dust masses in observed protoplanetary discs.

In Paper III, we conducted synthetic observations of discs, comparing how the total flux emitted from protoplanetary discs evolves with their apparent size. We examined how this relationship depends on the initial angular momentum of the cloud core from which the discs are created and on the efficiency of viscous heating. We found that discs with high angular momentum and weak viscous heating provide the best agreement with measurements of real discs. Additionally, we found that discs undergoing radial drift are generally optically thin.

Key words
Protoplanetary discs; Accretion discs; Planet formation

Classification system and/or index terms (if any)

Supplementary bibliographical information		**Language** English
ISSN and key title		**ISBN** ISBN: 978-91-8039-898-5 (print) ISBN: 978-91-8039-898-2 (pdf)
Recipient's notes	**Number of pages** 119	Price
	Security classification	

Signature Date 2024-01-26

Formation and Evolution of Protoplanetary Discs

Johan Appelgren

LUND
UNIVERSITY

Faculty Opponent

Dr. Paola Pinilla
Department of Space and Climate Physics, University College London,
London, England

Evaluation Committee

Dr. Stefano Facchini
Dipartimento di Fisic, Università degli Studi di Milano,
Milano, Italy

Docent David Hobbs
Department of Physics, Lund University,
Lund, Sweden

Docent Jouni Kainulainen
Department of Space, Earth and Environment,
Chalmers University of Technology,
Gothenburg, Sweden

Front cover: Appearing as a bird in flight, with wings outstretched in the expanse of space, the front cover shows the young star SU Aur. It is surrounded by a protoplanetary disc with long dust tails, and it is believed that the nebula is still feeding material to the disc. The image is captured by the SPHERE instrument on ESO's Very Large Telescope in Chile. Credit: ESO/Ginski et al.

Funding information: This thesis work has been financially supported by the Swedish Research Council grant (2018-04867, PI A. Johansen) and by the Wallenberg Academy Fellow grant (2017.0287, PI A. Johansen).

Faculty of Science, Department of Physics

ISBN: 978-91-8039-898-5 (print)
ISBN: 978-91-8039-899-2 (pdf)

Printed in Sweden by Media-Tryck, Lund University, Lund 2024

Contents

List of publications

This thesis is based on the following peer-reviewed publications:

I **Dust clearing by radial drift in protoplanetary discs**
J. Appelgren, M. Lambrechts, and A. Johansen (2020)
Astronomy & Astrophysics, Volume 638, id.A156, 17 pp.

II **Disc population synthesis: decrease of the solid mass reservoir through pebble drift**
J. Appelgren, M. Lambrechts, and N. van der Marel (2023)
Astronomy & Astrophysics, Volume 673 id.A139, 15 pp.

III **The evolution of the flux-size relationship in protoplanetary discs by viscous evolution and radial pebble drift**
J. Appelgren, A. Johansen, M. Lambrechts, J. Jørgensen, and N. van der Marel (2024)
To be submitted for publication.

Work not included in the thesis

Peer-reviewed publications not included in this thesis:

I **A Potential Site for Wide-orbit Giant Planet Formation in the IM Lup Disk**
A. D. Bosman, **J. Appelgren**, E. A. Bergin, M. Lambrechts, and A. Johansen (2023)
The Astrophysical Journal Letters, Volume 944, id.L53, 9 pp.

II **The formation of wide-orbit giant planets in protoplanetary disks with a decreasing pebble flux**
N. Gurrutxaga, M. Lambrechts, A. Johansen and **J. Appelgren** (2024)
Forthcoming publication in Astronomy & Astrophysics

"I knew exactly what to do,
but in a much more real sense,
I had no idea what to do."

– Michael Scott

Popular summary

For most of human existence, the list of known planets was limited to Earth and the other five solar system planets visible to the naked eye: Mercury, Venus, Mars, Jupiter, and Saturn. With the advent of astronomical telescopes, Uranus was discovered in 1781 by William Herschel, followed by the discovery of Neptune in 1846, along with numerous moons and dwarf planets.

The existence of planets around stars other than the Sun has been a subject of speculation for centuries. One of the earliest proponents, if not the first, was the 16th-century Italian philosopher Giordano Bruno. He wrote about an infinite universe and a plurality of worlds, suggesting the possibility of planets orbiting other stars. However, such ideas were not well-received by the Catholic Church of that era and may have played a role in Bruno's execution for heresy."

Time, however, would prove Giordano's ideas about other planets around other stars true. The first confirmed detection of a planet orbiting another star than our own, i.e. an exoplanet, was made in 1995. Swiss astrophysicist Michel Mayor and Didier Queloz discovered a planet similar in size to Jupiter orbiting the star 51 Pegasi, and thus named the planet 51 Pegasi b (implying that the star would be "a" in the system). This detection revolutionized planetary sciences, not only because it was the first exoplanet but also because it was a planet unlike any in the Solar system. While similar in size to Jupiter, 51 Pegasi b orbits its star 100 times closer than Jupiter orbits the Sun, even 8 times closer than Mercury orbits the Sun. Because it is so close to its stars, it is also very hot at just over 1000°C. This type of planet, of which many more have now been found, is now called a hot Jupiter.

Since this initial discovery, we have now identified over 5000 exoplanets. Following the pattern set by the first detection, a significant number of these exoplanets do not resemble those found in the Solar System. The most common category is the so-called Super-Earth, a planet with a size and mass falling between that of Earth and Neptune

This explosion in the number of known planets has challenged astronomers that try to explain how these planets form. While we before might have been content with explaining the formation of the types of planets found in the Solar system, we now also strive to explain the origins of the great diversity of exoplanets.

It appears natural that the diversity of discovered planets is intricately linked to the environments where these planets formed, known as protoplanetary discs. These discs and are found around the very youngest stars in the Universe, created from the gravitational collapse of enormous clouds of gas and dust. Some of this

material will settle into a disc surrounding the emerging star. Over time, the dust will grow from micrometer grains to mm-cm-sized pebbles. These pebbles move inwards through the disc, and some of them will be the building blocks of planets.

The quantity pebbles that can be supplied plays an important role in the outcome of planets formation. Abundant pebbles result in large cores of giant planets that eventually accrete massive gas atmosphere, forming the planets known as gas giants. A more limited supply of pebbles can result in the formation of planets that are unable to accrete significant amounts of gas, and end up as Super-Earth and terrestrial planets.

In this thesis, I have studied the evolution of the gas and dust in protoplanetary discs. I have examined how well the picture of dust grains growing into pebbles agrees with the observational data that has been collected on protoplanetary discs. The whole process from a disc forming together with a star to dust growing into pebbles, which eventually turn into planets, only takes a few million years. I write only because, by astrophysical standards, this is a very fast process. By the standards of a human life, it is, of course, very, very long. Even with the best modern observational techniques, we are only able to get short snapshots in time of real protoplanetary discs. If we want to study how a disc evolves from start to finish, we, therefore, have to use computer simulations where we can speed up time because the Universe is too slow and a human life is too short.

With this method, I have found that our theoretical understanding of the growth and radial drift of dust in protoplanetary discs agrees well with the data from real discs. This lends support to planet formation models where drifting pebbles are the building blocks of planets.

Populärvetenskaplig sammanfattning

Under stora delar av mänsklighetens historia har kännedomen av planeter varit begränsad till Jorden och de fem andra planeterna i solsystemet som går att se med blotta ögat – Merkurius, Venus, Mars, Jupiter och Saturnus. När de första teleskopen riktades mot himlen upptäcktes ett par till, nämligen Uranus år 1781 och Neptunus år 1846. Utöver dessa har det även upptäckts en stor mängd månar och dvärgplaneter i solsystemet.

Det har länge spekulerats kring om det kan finnas andra planeter än dem i solsystemet. En av de första personerna att förslå detta var den italienska 1500-tals filosofen Giordani Bruno. Han skrev redan då om ett oändligt universum och en mångfald av planeter kring andra stjärnor än solen. Den här typen av idéer var dessvärre inte så populära med katolska kyrkan på den tiden, och bidrog till att han avrättades för kätteri.

Med tiden kom Giordanis tankar om planeter kring främmande stjärnor emellertid att bevisas. En planet som med säkerhet bekräftades kring en stjärna som inte är solen, en så kallad exoplanet, upptäcktes år 1995. De schweiziska astrofysikerna Michel Mayor och Didier Queloz upptäckte en planet kring stjärnor Pegasi 51, och döpte planeten till 51 Pegasi b (själva stjärnan anses vara Pegasi 51 a). Denna upptäckt innebar en revolution för astronomin, inte bara för att det var den första exoplaneten som upptäcktes, men och för att det var en planet olik någon av solsystemets planeter. Visserligen är den ungefär stor som Jupiter, men dess omloppsbana ligger 100 gånger närmare sin stjärna än Jupiters, det vill säga ca 8 gånger närmare än Merkurius bana. Eftersom 51 Pegasi b ligger så pass nära sin stjärna är den också väldigt varm, strax över 1000° C. Denna typ av planet kallas därför en ”het Jupiter”.

Sedan denna första upptäckt har man funnit över 5000 exoplaneter. I likhet med den första upptäckten, har det visat sig att många av dessa planeter skiljer sig signifikant från dem i solsystemet. Den vanligaste typen av planet har visat sig vara en så kallad super-Jord. Dessa planeter har massor och storlekar som ligger mellan Jorden och Neptunus.

Denna, nästan lavinartade, ökning i antalet kända planeter, tillsammans med variationen bland dessa, har utmanat astrofysiker till att utveckla sina teorier kring hur planeter bildas. Medan man förr kanske hade nöjt sig med att bara förklara hur solsystemets planeter bildades, så räckte detta inte längre.

Det är rimligt att anta att en del av variationen bland exoplaneter skulle kunna förklaras med skillnader bland de miljöer planeterna bildas i. Dessa miljöer kallas protoplanetära skivor och är skivor av gas och stoft som omger de allra yngsta

stjärnorna i universum. När dessa stjärnor bildas från kollapsande moln kommer en del av gasen och stoftet landa i en skiva som omringar stjärnan. Med tiden kommer stoftet i skivan växa till mm-cm stora småstenar som driver inåt genom skivan, mot stjärnan. Dessa småstenar utgör de byggstenar som planeter bildas från.

Hur mycket av dessa småstenar som finns kan avgöra vilken typ av planet bildas – finns det många småstenar är det troligare att det bildas stora planeter som till slut kan dra till sig enorma mängder gas, och bilda gasjättar. Finns det färre småstenar så resulterar det i mindre planeter, exempelvis en super-Jord.

I denna avhandling har jag studerat hur dessa protoplanetära skivor utvecklas. Jag har undersökt hur vår bild av stoft som växer till småstenar och sedan driver genom skivan stämmer med den data om protoplanetära skivor som samlats in från världens största teleskop. Hela processen att gå från att en protoplanetär skiva bildas till att planeter tar form tar några miljoner år. Det må låta som en lång tid, men med astronomiska mått mätt är det faktiskt en rätt snabb process. Det är ju dock ofantligt mycket längre än en mänsklig livstid. Därför kan våra observationer av protoplanetära skivor bara låta oss se ett enskilt ögonblick av dess livstid. Genom att observera många skivor av olika åldrar kan vi förbättra vår förståelse, men om vi vill följa en skivas utveckling från början till slut måste vi använda oss av datorsimuleringar. Dessa låter oss snabbspola fram i tiden, och studera miljontals år av utveckling, och på så sätt överkomma våra korta liv.

Med dessa metoder har jag funnit att den teoretiska bilden av hur stoftet i protoplanetära skivor växer och driver genom skivan stämmer överens bra med datan från verkliga skivor. Detta i sin tur ger bra stöd åt de modeller för hur planeter bildas som bygger på att det är dessa drivande småstenar som är planeternas byggstenar.

Acknowledgements

Firstly, I would like to thank my supervisor, Anders, for giving me the opportunity to undertake this PhD project, and his support throughout it. I am also very thankful to Michiel for his scientific mentoring, advice, and the many fun moments we shared. I want to thank Nienke van der Marel for her advice and support, especially on the observational aspects of protoplanetary discs.

I want to thank all friends I've made at Lund Observatory for the many great moments we have shared. Special thanks to Ross and Santi for all the hikes we have made together. Thank you also to Alvaro for all the great table tennis matches and the fantastic tournaments.

Thank you to Eva for dealing with all those tedious administrative task that I cannot stand, and for helping with anything I asked. Thank you to Anna for giving me the opportunity to spend so much time in the planetarium. The opportunity to communicate science this way was both a very valuable and cool experience.

I give my deepest thanks and gratitude to my wonderful Rebecca. Without you this project would never have been finished. Thank you for all your support and for believing in me, even in moments when I did not. I am also incredibly thankful for all your help with this thesis - your advice and comments on the text and for telling me about all the things that are necessary necessary in the final months that no-one else seems to know.

Lastly, I want to thank my family for their continuous support and belief in me over the years.

Part I

Research context

Summary of Scientific Publications

My thesis concerns the evolution of protoplanetary discs, with a focus on the evolution of the dust component through radial drift. I have studied this by developing a numerical model that incorporates disc formation, viscous evolution, photoevaporation of the gas, and radial drift of dust pebbles.

The work in this thesis employs a population synthesis approach to model disc evolution across a wide range of stellar and disc masses. This approach enables us to compare our model with observed dust evolution trends. Below, I summarize the content of each article in this thesis.

Paper I: *Dust clearing by radial drift on evolving protoplanetary discs*
We study the evolution of protoplanetary discs forming from the gravitational collapse of a molecular cloud core. The gas discs continue to evolve as viscous accretion discs, while the dust evolves through radial drift, constrained in size to 100 μm as suggested by polarized light from protoplanetary discs. We study how the mass and angular momentum of the cloud core affects disc evolution and make a population synthesis study. With this we investigate the evolution of the dust disc mass and scaling relationships with the stellar mass.

Paper II: *Disc population synthesis: decrease of the solid mass reservoir through pebble drift*
We build upon the model of the previous paper to include dust particle sizes limited by fragmentation and accounting for gas disc dispersal through photoevaporation. Additionally, we also model he temperature of the disc, taking into account stellar irradiation and viscous heating. We model synthetic populations of discs evolving under different viscous alphas, and dispersing through strong X-ray evaporation or less efficient FUV evaporation. We find that the temporal evolution of the cumulative distribution of dust disc masses in our model agrees well with that observed in nearby star-forming regions.

Paper III: *The evolution of the flux-size relationship in protoplanetary discs by viscous evolution and radial pebble drift*
In this paper, we calculate the fluxes and flux radii of evolving protoplanetary dust discs using the model of the second paper. We study how the relationship between the flux and the flux radius evolve over time and compare to observational measurement of protoplanetary discs. We examine the effects of viscous heating and cloud core angular momentum and find that discs with weak viscous heating and high angular momentum is most able to reproduce the observed fluxes and flux radii.

Chapter 1

Protoplanetary disc formation and evolution

In the past three decades, a fundamental shift in our understanding of planets has taken place. Our initial inventory of planets was limited to the terrestrial planets in the inner Solar system and the gas giants and ice giants of the outer Solar system. However, the very first exoplanet discovered around a Sun-like star proved to be a gas giant with a very close-in semi-major axis of 0.05 au (Mayor & Queloz, 1995), a type of planet now referred to as a hot Jupiter. While the detection of exoplanets, especially those similar to the Solar system planets, is still very much limited by both technological and time constraints, the continued search for exoplanets have revealed a diversity of planets not seen in the Solar system. A very common type of planet are the so-called super-Earths, found around at least 30% of Sun-like stars (Zhu et al., 2018). These mostly rocky planets have masses and radii between that of Earth and Neptune and have no analogue in the Solar system.

Models of planet formation have similarly seen significant development in the past decade. The core accretion scenario remains as the favoured model of giant planet formation (Pollack et al., 1996). In this scenario, the core of a giant planet first form by the accretion of rocky and icy material, and a gas envelope is then accreted from the protoplanetary disc. However, the formation of the cores of giant planets by planetesimal accretion at radii beyond 5 au takes more than 10^7 yr, longer than typical disc lifetimes of 10^{6-7} yr. Models of giant planet formation based on the accretion of mm-cm-sized pebbles rather than planetesimals were therefore developed (Johansen & Lacerda, 2010; Ormel & Klahr, 2010). The timescale of pebble accretion is much shorter than those of planetesimal accretion,

allowing for the rapid formation of the cores of giant planets at wide orbits (Lambrechts & Johansen, 2012; Gurrutxaga et al., 2024). Pebble accretion has also been shown to be capable of forming super-Earths and terrestrial planets (Ormel et al., 2017; Lambrechts et al., 2019; Johansen et al., 2021). Development of pure planetesimal accretion models have also shown that these are able to form super-Earths from rings of planetesimals, which themselves are created from rings pebbles (Batygin & Morbidelli, 2023). Such rings and other substructures have been observed in several protoplanetary discs (e.g. Andrews et al., 2018). However, if these substructures are the result of, or the preface too, planet formation, or caused by other mechanisms is still not clear (Pinilla et al., 2017, 2020).

The diversity of exoplanets likely reflects a diversity in the environments, and possibly the physical mechanism, that formed the planets. As an example, the occurrence rate of giant planets has been found to be more common around stars with a higher metallicity, i.e. a higher abundance of heavier elements, in several studies (Fischer & Valenti, 2005; Johnson et al., 2010; Fulton et al., 2021), suggesting a more efficient formation of giant planets in protoplanetary discs with high dust-to-gas ratios. Understanding the evolution of protoplanetary discs, and how it varies with stellar mass and disc mass is crucial if we wish to understand how the diverse range of exoplanets that we observe came to be.

In this chapter, I focus on our theoretical understanding of the main drivers of protoplanetary disc evolution. I will cover the classification of the evolutionary stages of protoplanetary disc, a model of disc formation, the drivers of gas and dust disc evolution and the final dispersal of protoplanetary discs.

1.1 Evolutionary stages

Young stellar objects (YSOs) are the very youngest stars and their surrounding discs. Identification of a YSO is possible because its spectral energy distribution (SED) is different from that of a star due to an excess of infrared emission, originating from the cooler dust in the envelope and disc around the protostar. The resulting SED is the sum of the individual black body radiation of the star and disc. As the envelope dissipates and the disc evolves and eventually disperses, the SED will change due to the shift in the excess infrared emission from the disc. YSOs are classified into one of four groups, class 0, I, II, and III. Each class reflects a different stage of disc evolution, with class 0 objects being the youngest. The classification is made from the slope of the SED in the mid-infrared ($\lambda = 2-20\ \mu$m),

given by

$$\alpha_{\rm IR} = \frac{{\rm d}\log(\lambda F_\lambda)}{{\rm d}\log\lambda}, \tag{1.1}$$

where λ is the observing wavelength and F_λ the flux at this wavelength. The classification of young stellar objects into class I, II, and III was originally proposed by Lada (1987), with the class 0 group being added later by Greene et al. (1994). In this thesis, I have studied all stages of the evolution of protoplanetary disc, from formation at class 0 to the dispersion at class III, and below follows a description of the different stages.

Class 0 objects are the youngest objects, representing the first stages of star formation. In these objects, a central core sits deeply embedded within a surrounding envelope of gas and dust. The envelope accretes onto the core, forming a protostar and surrounding disc. Class 0 objects are defined by the absence of excess emission at $\lambda < 20$ μm, which is missing due to the lack of black-body radiation from the not-yet-formed protostar.

Class I objects are also embedded in and accreting from the envelope, but by this stage, a protostar and disc have formed. The resulting SED is a combination of the radiation from the star and a large contribution from the colder disc. This results in significant emission in excess of the protostar's black-body radiation in the mid-infrared. Class I objects have $\alpha > 0.3$. Together, the class 0 and I stages last $\sim$0.5 Myr.

The class II stage has fully formed protoplanetary discs, with a mass that is about 1 % of the stellar mass. Over a timescale of a few million years, the dust and gas of the disc will disperse through several possible mechanisms. The final clearing of the gas disc likely occurs through photoevaporation, as viscous evolution on its own is too slow to clear the disc within reasonable timescales. The dust is removed from the disc by radial drift and the incorporation into planetesimals and planets. These discs also have an excess of mid-infrared emission, but not as significant as the class I objects. Class II objects have $-1.6 < \alpha < -0.3$. The class II stage of disc evolution is expected to last up to several million years.

By the class III, the disc is almost completely cleared, and minimal accretion onto the star occurs. Due to the lack of a significant disc, the SED is dominated by the stellar component. These objects have $\alpha < -1.6$ and can be distinguished from main sequence stars by being more luminous.

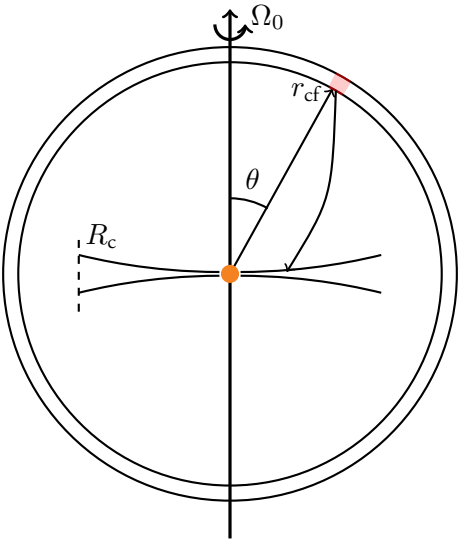

Figure 1.1: Illustration of the gravitational collapse of one spherical shell of the molecular cloud core. The cloud core rotates with an angular frequency of Ω_0. A parcel of gas at radius $r_{\rm cf}$ from the center and angle θ from the rotational axis will collapse under the conservation of angular momentum. A parcel of gas with $\theta = 90°$ will land the furthest out in the disc at the centrifugal radius $R_{\rm c}$.

1.2 Disc formation

Protoplanetary discs and the stars that they surround form by the gravitational collapse of cold and dense molecular cloud cores. Typical core temperatures are 10-20 K, and densities are orders of magnitude higher than that of the surrounding molecular cloud (McKee & Ostriker, 2007; Pineda et al., 2023). If the cloud core is dense enough that the self-gravity is stronger than the pressure support, it will collapse. Cloud cores rotate at some angular frequency Ω_0, and conservation of angular momentum dictates that a fraction of the gas and dust will settle into a disc around the protostar. An illustration of the gravitational collapse of a molecular cloud core is shown in Fig. 1.1. In this view of star and disc formation, the collapse proceeds inside-out, with the collapse starting at the center of the core, and a collapse front expanding outwards until it reaches the outer edge of the cloud core. An example of a molecular cloud core is Barnard 68, shown in Fig. 1.2. Barnard 68 measures approximately 12,500 au across, or 0.2 light years, and has

a temperature ranging from 16 K at the outer edge to 8 K at the center (Nielbock et al., 2012). It is believed that Barnard 68 will collapse into a low-mass star within the next 0.2 Myr (Burkert & Alves, 2009).

The structure of a spherical gas cloud under hydrostatic equilibrium can be described by the Lane-Emden equation given by

$$\frac{1}{r^2}\frac{\mathrm{d}}{\mathrm{d}r}\left(\frac{r^2}{\rho}\frac{\mathrm{d}\rho}{\mathrm{d}r}\right) = -\frac{4\pi G\rho}{c_\mathrm{s}^2}, \tag{1.2}$$

where r is the radial position in the cloud, ρ is the density, and c_s is the sound speed. A simple solution to this equation exists as

$$\rho\left(r\right) = \frac{c_\mathrm{s}^2}{2\pi G r^2}. \tag{1.3}$$

This solution has a singularity at the center, i.e., $\rho \to \infty$ as $r \to 0$, and is therefore known as the singular isothermal sphere (Shu, 1977). One of the features of a singular isothermal sphere as a cloud core model is that it results in an infall rate that is constant over time.

A solution to the Lane-Emden equation which does not have a singularity at the center is that of a Bonnor-Ebert sphere (Bonnor, 1956; Ebert, 1957). Imposed upon this sphere are the boundary conditions that the density in the middle must be finite such that $\rho(0) = \rho_\mathrm{c}$, and that the density at the center is differentiable and has an extremum at this point. It has been found that several real cloud cores, such as the one shown in Figure 1.2, have density structures that are similar to that of a Bonnor-Ebert sphere (Alves et al., 2001; Teixeira et al., 2005; Kandori et al., 2005; Kirk et al., 2005).

There exists no analytical solution for the density of a Bonnor-Ebert sphere, and the density must be found numerically. We start by defining a typical length scale of a Bonnor-Ebert sphere as

$$r_\mathrm{c} = \frac{c_\mathrm{s}^2}{4\pi G\rho_\mathrm{c}}. \tag{1.4}$$

We then further define the dimensionless density and distance parameters ϕ and ξ as

$$\phi = \ln(\rho/\rho_\mathrm{c}), \tag{1.5}$$

$$\xi = r/r_\mathrm{c}. \tag{1.6}$$

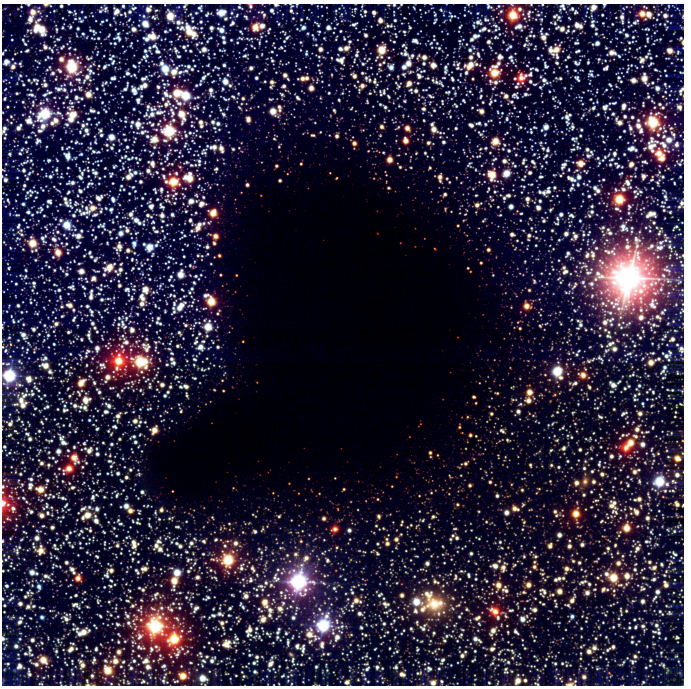

Figure 1.2: Barnard 68 is a molecular cloud core appearing as dark patch on the sky by absorbing background emission. It is on the verge of gravitational collapse, which would trigger star and disc formation. Credit: ESO.

With these dimensionless parameters, the Land-Emden equation has the form of

$$\frac{1}{\xi}\frac{\mathrm{d}}{\mathrm{d}\xi}\left(\xi^2\frac{\mathrm{d}\phi}{\mathrm{d}\xi}\right)+e^{\phi}=0. \tag{1.7}$$

and the boundary conditions of a Bonner-Ebert sphere is $\phi(0)=0$ and $\phi'(0)=0$. This equation can be solved as a system of two coupled first-order equations given by

$$\frac{\mathrm{d}\phi}{\mathrm{d}\xi}=\frac{u}{\xi^2}, \tag{1.8}$$

$$\frac{\mathrm{d}u}{\mathrm{d}\xi}=-\xi^2 e^{\phi}, \tag{1.9}$$

with the boundary conditions that $\phi(0)=0$ and $u(0)=0$.

From the equations of motion, the total acceleration that a collapsing shell experiences is given by

$$\frac{\mathrm{D}u}{\mathrm{D}t} = -\frac{c_\mathrm{s}^2}{\rho}\frac{\partial \rho}{\partial r} - \frac{GM_\mathrm{in}}{r^2} \tag{1.10}$$

$$= \frac{c_\mathrm{s}^2}{r}F(r) - \frac{GM_\mathrm{in}}{r^2}, \tag{1.11}$$

where r is the radius in the cloud core, and M_in is the mass interior to this radius. A collapsing shell spends most of its time at radii far from the centre, therefore the value of the function $F(r) = (r/\rho)\partial\rho/\partial r$ can be approximated as its initial position in the cloud core, r_ini. In hydrostatic equilibrium F is given by

$$F(r_\mathrm{ini}) = \frac{GM_\mathrm{in}}{f c_\mathrm{s}^2 r_\mathrm{ini}}, \tag{1.12}$$

where f is a factor by which the density of the cloud core is increased over that of a standard Bonnor-Ebert sphere, in order to trigger gravitational collapse. Using Equation (1.11) and (1.12), one can find the velocity of a collapsing shell, which in turn gives the timescale for the collapse a Bonnor-Ebert sphere can be found as

$$t_\mathrm{collapse} = \sqrt{\frac{r_\mathrm{BE}^3}{2GM_\mathrm{BE}}}\int_0^R \frac{\mathrm{d}R}{\sqrt{\frac{1}{f}\ln R + \frac{1}{R} - 1}}, \tag{1.13}$$

where r_BE is the radius of the cloud core, M_BE is the mass of the cloud core, and $R = r/r_\mathrm{BE}$ (Takahashi et al., 2013). Unlike the singular isothermal sphere model, the infall rate of gas onto the star and disc from a Bonnor-Ebert sphere is not constant in time and is given by

$$\dot{M}_\mathrm{g}(t) = 4\pi\rho r_\mathrm{cf}^2\frac{\mathrm{d}r_\mathrm{cf}}{\mathrm{d}t}. \tag{1.14}$$

The last term of the equation describes the velocity that the collapse front radius, r_cf, expands outwards at and is given by

$$\frac{\mathrm{d}r_\mathrm{cf}}{\mathrm{d}t} = \frac{2r_\mathrm{cf}\beta^2}{3t\beta^2 - 2\pi t^3\rho(r_\mathrm{cf})}. \tag{1.15}$$

Equation (1.15) can be found from equation (1.13) where β is given by

$$\beta = \sqrt{\frac{1}{2G}} \int_0^R \frac{\mathrm{d}R}{\sqrt{\frac{1}{f}\ln R + \frac{1}{R} - 1}}. \tag{1.16}$$

The infall rate of gas onto a position r in the disc from an angle of θ in the cloud core is given by

$$\frac{\partial \dot{M}_\mathrm{g}}{\partial r} = 2\frac{\partial \dot{M}_\mathrm{g}}{\partial \theta}\frac{\partial \theta}{\partial j}\frac{\partial j}{\partial r}, \tag{1.17}$$

where the factor 2 comes from the fact that mass falls onto the disc from two sides, and j is the specific angular momentum of the gas. The mass of a parcel of gas is given by

$$\mathrm{d}M_\mathrm{g} = 2\pi\rho \sin\theta r_\mathrm{cf}^2 \,\mathrm{d}\theta \mathrm{d}r_\mathrm{cf}. \tag{1.18}$$

Differentiating this with respect to t, one can find the mass infall rate per unit angle as

$$\frac{\partial \dot{M}_\mathrm{g}}{\partial \theta} = \frac{\dot{M}_\mathrm{g}}{2}\sin\theta. \tag{1.19}$$

From conservation of angular momentum, we can equate the specific angular momentum in the cloud with that in the disc

$$j = \left(r_\mathrm{cf}\sin\theta\right)^2 \Omega_0 = \left(GMr\right)^{1/2}, \tag{1.20}$$

where M is the mass in the disc contained within r, or equivalently, the mass in the cloud contained within r_cf. We can find the maximum radius at which gas will land in the disc from Equation (1.20) by setting $\theta = 90°$. This is called the centrifugal radius and is given by

$$R_\mathrm{c}\left(r_\mathrm{cf}\right) = \frac{\Omega_0^2 r_\mathrm{cf}^4}{M(r_\mathrm{cf})\,G}. \tag{1.21}$$

By setting $r_\mathrm{cf} = r_\mathrm{BE}$ one finds the maximum radius at which any infalling material will land. Using equations (1.19), (1.14), and (1.20), equation (1.17) can be expressed in a surface density form in terms of r and R_C as

$$\frac{\partial \Sigma_\mathrm{g,inf}}{\partial t} = \frac{\dot{M}_\mathrm{g}}{8\pi R_\mathrm{c}^2}\left(\frac{r}{R_\mathrm{c}}\right)^{-3/2}\left[1 - \left(\frac{r}{R_\mathrm{c}}\right)^{1/2}\right]^{-1/2}. \tag{1.22}$$

1.3 Protoplanetary disc as accretion discs

One of the fundamental processes ongoing in protoplanetary discs is the accretion of gas from the disc onto the star. Accretion onto protostars is inferred from an excess luminosity originating from the hotspots on the stellar surface where the accreted material lands. Accretion rates measured from the accretion luminosity have revealed that the rate of accretion span several orders of magnitude from $10^{-7}\ M_{\odot}\ \mathrm{yr}^{-1}$ to $10^{-12}\ M_{\odot}\ \mathrm{yr}^{-1}$ (Hartmann et al., 1998; Gullbring et al., 1998; Herczeg & Hillenbrand, 2008; Ingleby et al., 2013; Alcalá et al., 2014, 2017; Manara et al., 2017). In order for gas to be both transported to the inner disc edge and to be accreted onto the star it must lose angular momentum. The physical mechanism that causes the gas to lose angular momentum is not fully understood. The two main proposed mechanisms are the viscous redistribution of angular momentum and the removal of angular momentum by magnetic disc winds.

Protoplanetary discs as viscous accretion discs

In a viscous accretion disc, angular momentum is redistributed by viscosity acting on shear from the differential rotation of neighbouring annuli of gas in the disc. The effectiveness of the redistribution of angular momentum is determined by the viscosity of the disc. In this process, most of the mass is transported inwards, and the angular momentum is deposited in a small fraction of the mass that moves outwards. The temporal evolution of a viscous accretion disc is therefore characterised by a disc with decreasing mass but increasing size. Originally, the proposed source of viscosity was molecular viscosity, but this is not strong enough to generate the accretion rates measured onto protostars and to drive disc evolution on short-enough timescales. Instead, turbulence has been proposed as the source of disc viscosity (Lynden-Bell & Pringle, 1974). However, finding a physical mechanism strong enough to generate sufficient turbulence to explain observed accretion rates has proven difficult.

A proposed mechanism to drive disc turbulence is the magneto-rotational instability (MRI) discovered by Balbus & Hawley (1991). This instability exists in weakly magnetised discs, with outwardly decreasing rotational velocity, under conditions of ideal magneto-hydrodynamics (MHD). If the MRI is active, the resulting turbulent viscosity is able to drive accretion rates high enough to explain observed rates. However, it has been found that only the thermally ionised inner regions and the cosmic ray ionised outer regions of protoplanetary discs are magnetised enough for the MRI to be active. Between these regions, non-ideal MHD

conditions have to be taken into account. These have been found to weaken or suppress the MRI (Bai & Stone, 2013).

Despite the lack of an understanding of the drivers of disc turbulence, the viscous accretion disc model is still frequently used due to its ease of implementation and ability to explain several of the observed disc features. With the argument that the size of turbulent eddies is naturally limited by the scale height of the gas disc $H_{\rm g}$, and that the turbulent speed in the eddies is limited by the sound speed $c_{\rm s}$, the viscosity of an accretion disc can be parameterised with a scaling parameter $\alpha < 1$. From this, one arrives at the famous α-disc model of Shakura & Sunyaev (1973) for the viscosity of an accretion disc, given by

$$\nu = \alpha H_{\rm g} c_{\rm s}. \tag{1.23}$$

Modelling of the viscous evolution of the gas discs can be done by combining the continuity equation with the equations for the conservation of angular momentum. Pringle (1981) showed that these two equations can be combined into one single equation for determining viscous disc evolution:

$$\frac{\partial \Sigma_{\rm g}}{\partial r} = \frac{3}{r}\frac{\partial}{\partial r}\left[r^{1/2}\frac{\partial}{\partial r}\left(\nu \Sigma_{\rm g} r^{1/2}\right)\right]. \tag{1.24}$$

The evolution of a protoplanetary gas disc undergoing formation and viscous accretion is shown in Fig. 1.3. The disc temperature is set by irradiation and viscous heating. As seen, the inner disc is drained of gas whilst the outer disc expands as a small fraction of the gas gains angular momentum and moves outwards. The dashed lines show the same model but including dispersal of the disc by photoevaporation, discussed more in Section 1.7.

Protoplanetary discs as wind driven accretion discs

In the past decade, it has been realised that the gas in protoplanetary discs is likely to be very weakly ionised. Under such conditions, non-ideal MHD effects have to be taken into consideration. In the presence of a vertical magnetic field, ambipolar diffusion suppresses the MRI in the inner regions of the protoplanetary disc. Angular momentum is instead carried away by a wind launched at the surface of the disc (Bai & Stone, 2013; Bai, 2013).

In wind driven accretion, the effect of the vertical magnetic field on the gas disc is that a breaking torque acts on the inside the disc and an accelerating torque at the discs surface. This process removes angular momentum from the gas in the

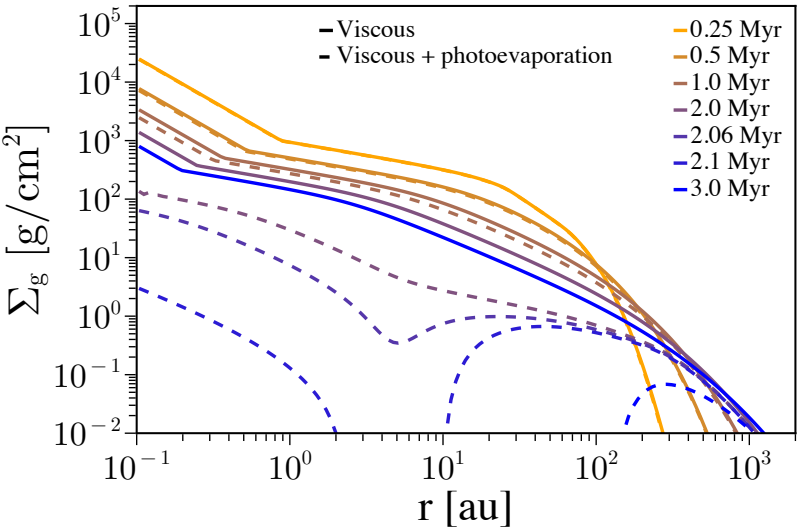

Figure 1.3: Evolution of a gas disc from the disc model developed in this thesis. The disc forms from the collapse of a 1 $M_\odot$ Bonnor-Ebert sphere with a centrifugal radius of 10 au. Subsequent viscous evolution occurs under $\alpha_\nu = 10^{-2}$. The dashed lines show the same model but also includes disc dispersal with the X-ray photoevaporation prescription of (Picogna et al., 2021).

disc midplane, resulting in accretion of gas. The angular momentum is transported to the surface of the disc, where the acceleration of the gas leads to its ejection from the disc. Magnetic disc winds thus remove both angular momentum and gas from the disc. The disc accretion rate in wind driven discs at radii of about 10 au has been found to be similar to the accretion rate in observed disc (Bai, 2017).

The accretion rate that wind-driven discs are able to achieve depends primarily on the strength of the magnetic field (Pascucci et al., 2023). This magnetic field is inherited from the molecular cloud core. Observational studies of the strength and structure of the magnetic field in protoplanetary discs have been made, but it is generally poorly constrained (e.g., Vlemmings et al., 2019; Teague et al., 2021).

Because purely wind-driven discs have no radial transport of angular momentum, they are expected to shrink with time rather than to expand, as a viscously driven disc does. This could potentially be used to observationally separate wind-driven discs from viscously driven discs. However, global non-ideal MHD simulations of protoplanetary discs have shown that expansion can occur also in wind-

driven discs (Yang & Bai, 2021). This is further complicated by the outer discs possibly being MRI active due to cosmic ray ionisation, allowing for radial angular momentum transport.

1.4 Radial drift of dust particles

One of the basic physical processes that affects dust in protoplanetary discs is radial drift, illustrated in Figure 1.4. Radial drift is the inwards motion of dust particles caused by the loss of angular momentum due to azimuthal gas drag. The origin of the gas drag is the radial pressure gradient present in the disc. This pressure gradient exerts an outwards acting force on the gas but, crucially, not the dust, adding additional support against the gravitational force of the star. The centrifugal force can, therefore, be weaker than for a pure Keplerian orbit, and the gas orbits at a sub-Keplerian speed, given by (Weidenschilling, 1977; Nakagawa et al., 1986)

$$v_\phi = v_\mathrm{K}\left(1-\eta\right), \tag{1.25}$$

where $v_\mathrm{K} = \sqrt{GM_\star/r}$ is the Keplerian orbital speed and η is a dimensionless pressure gradient parameter. It is given by

$$\eta = -\frac{1}{2}\left(\frac{H}{r}\right)^2 \frac{\partial \ln P}{\partial \ln r}, \tag{1.26}$$

where P is the disc midplane pressure. Since the dust does not feel the pressure gradient support, it will orbit at a Keplerian speed. This difference in orbital speed results in the above-mentioned gas drag, and the inwards radial drift of dust.

How strongly a dust particle is affected by gas drag, and thus how fast radial drift will be, can be quantified with the dimensionless Stokes number, St. A particle with a Stokes number of 1 is drifting most efficiently. A particle with a Stokes number higher or lower than 1 will drift less efficiently. In the limit where the Stokes number approaches 0, a dust particle is fully coupled to the gas. The motions of strongly coupled particles ($\mathrm{St} \lesssim 0.01$) particles are heavily affected by advection with the gas. At Stokes number greater than 1 particles begin to completely decouple from the gas and their motions are unaffected by gas drag. The radial drift speed is given by (Nakagawa et al., 1986)

$$v_\mathrm{drift} = -\frac{2\mathrm{St}}{1+\mathrm{St}^2}\eta v_\mathrm{k}, \tag{1.27}$$

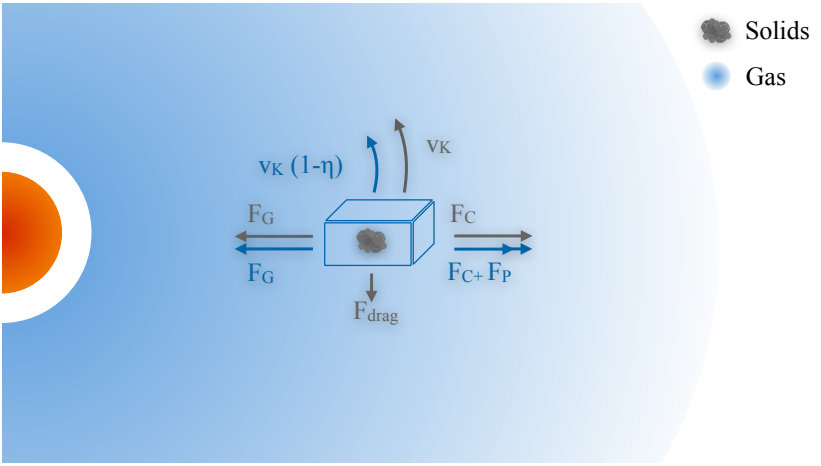

Figure 1.4: Illustration of the physical mechanism behind radial drift of dust particles. A parcel of gas in the protoplanetary disc is supported against the gravitational force, $F_{\rm G}$, by both the centrifugal force, $F_{\rm C}$, and the pressure gradient, $F_{\rm P}$, in the disc. The degree of pressure support is determined by the dimensionless pressure support parameter η. Because of the reduced centrifugal force, the gas orbits at a sub-Keplerian velocity $v_{\rm K}\,(1-\eta)$. A dust particle does not feel the pressure gradient and therefore orbits at a Keplerian velocity, $v_{\rm k}$. This difference in orbital velocity results in a drag force on the dust, causing it to lose angular momentum and drift inwards in the disc.

where, $v_{\rm k}$ is the Keplerian orbital velocity.

The Stokes number of a particle depends on the properties of the particle itself and also on the environment it is found in. If the particle's size is smaller than the mean free path in the medium, the particle is in the Epstein regime. If the particle is larger than the mean free path, the particle is in the Stokes regime, which can occur in the innermost regions of the disc. The Stokes number is calculated with the following equation

$$\mathrm{St} = \begin{cases} \dfrac{\sqrt{2\pi}\rho_\bullet a_{\rm d}}{\Sigma_{\rm g}} & \text{if } a_{\rm d} < \dfrac{9}{4}\lambda_{\rm mfp}, \\ \dfrac{4}{9}\dfrac{a_{\rm d}}{\lambda_{\rm mfp}}\dfrac{\sqrt{2\pi}\rho_\bullet a_{\rm d}}{\Sigma_{\rm g}} & \text{if } a_{\rm d} \geq \dfrac{9}{4}\lambda_{\rm mfp}. \end{cases} \tag{1.28}$$

where $a_{\rm d}$ is the size of a dust particle, $\rho_\bullet$ is the material density of a dust particle, and $\lambda_{\rm mfp}$ is the mean free path. The density of dust grains in protoplanetary discs

is not known. In the regime of compact grains, a density of $\rho_\bullet = 1.6\,\mathrm{g\,cm^{-3}}$ is appropriate (Birnstiel et al., 2012). Dust grains are generally in the Epstein regime. The Stokes regime only occurs in the innermost regions of the disc, if dust grains grow very large.

The total velocity of the dust is given by the drift velocity combined with the advective velocity and is given by

$$v_{\mathrm{d,r}} = v_{\mathrm{drift}} + \frac{v_{\mathrm{g}}}{1 + \mathrm{St}^2}. \tag{1.29}$$

The evolution of the dust surface density due to radial drift and advection with the gas can be described by the following continuity equation

$$\frac{\partial \Sigma_{\mathrm{d}}}{\partial t} = -\frac{1}{r}\frac{\partial}{\partial r}\left(r \Sigma_{\mathrm{d}} v_{\mathrm{d,r}}\right). \tag{1.30}$$

1.5 Sizes of dust particles

In the interstellar medium dust particles have sub-micron sizes (Natta et al., 2007) and at the stage of class II discs, dust has grown through hitting and sticking into mm/cm sizes (e.g. Carrasco-González et al., 2019). The growth is thought to mainly occur in the protoplanetary disc. But, if the collapse of the molecular cloud core is slower than the free-fall timescale, growth of dust grain up a size of 100 μm is possible (Ormel et al., 2009). A dust particles continues to grow until it hit one of several potential barriers that can limit further growth.

The zoo of possible outcomes from dust particles collisions is very varied. However, a few of key outcomes limiting growth have been determined. The perhaps most important restriction on growth is the so-called fragmentation limit. In this limit, the collision of two particles is so energetic that the particles fragment into smaller components. As particles grow larger, the velocities in particle collisions increase and eventually reach the limit where collisions result in fragmentation. The velocity this occurs at is the fragmentation velocity, v_{f}, and is a key parameter for dust disc evolution. The value of v_{f} depends on the material properties of the dust particles, and importantly on the monomer size of dust. It can therefore be different in cold disc regions where dust particles are icy, compared to hotter regions where ices have sublimated. Laboratory measurement of v_{f} have reveled that for silicate particles $v_{\mathrm{f}} \approx 1$ m/s (Blum & Münch, 1993; Blum & Wurm, 2008). Icy particles were long thought to be stickier and to have a higher fragmentation limit of $v_{\mathrm{f}} \approx 10$ m/s (Gundlach & Blum, 2015). However, it has

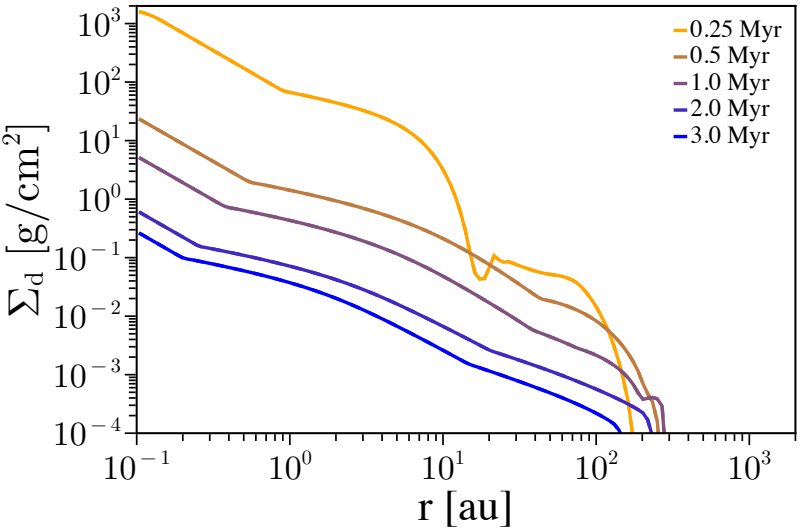

Figure 1.5: Evolution of the dust surface density, in the model developed in this thesis, of a disc forming from a 1 $M_\odot$ cloud core with a centrifugal radius of 10 au. Dust growth is limited by fragmentation at a velocity of 1 m/s and particle stirring at $\alpha_t = 10^{-4}$.

been shown that this might not be the case and that the fragmentation velocity of icy particles is similar to that of silicates (Musiolik et al., 2016a,b). A global fragmentation limit of 1 m/s should therefore be appropriate.

The particle size at which fragmentation occurs is given by (Birnstiel et al., 2012)

$$a_{\rm frag} = f_{\rm f} \frac{2}{3\pi} \frac{\Sigma_{\rm g}}{\rho_\bullet \alpha_{\rm t}} \frac{v_{\rm f}^2}{c_{\rm s}^2}, \tag{1.31}$$

where $f_{\rm f} = 0.37$ is a fudge factor, and $\alpha_{\rm t}$ is a measure of the mid-plane stirring, which is not necessarily the same as α_ν.

If particles are able to grow to such a size that the timescale for radial drift is shorter than the timescale for further growth, they are size-limited by the radial drift barrier. In this limit, the particle size is given by (Birnstiel et al., 2012)

$$a_{\rm drift} = f_{\rm d} \frac{2\Sigma_{\rm d}}{\pi \rho_\bullet} \frac{v_{\rm k}^2}{c_{\rm s}^2} \gamma^{-1}, \tag{1.32}$$

where $f_{\rm d} = 0.55$ is a fudge factor, and γ is the absolute value of the radial pressure gradient. From the relative velocities of grains under turbulent motion, the timescale for dust grains to grow from their initial micron sizes can be approximated by

$$t_{\rm grow} = \frac{\Sigma_{\rm g}}{\Sigma_{\rm d}\Omega_{\rm K}}, \tag{1.33}$$

where $\Omega_{\rm K}$ is the Keplerian orbital frequency. At a dust-to-gas ratio of 0.01, the growth timescale at 10 au around a solar-mass star is about 500 yr, even at 100 au, it is only about 16,000 yr. This is significantly shorter than disc lifetimes, and even shorter than the disc formation timescale (Eq. (1.13)). Dust sizes are therefore only limited by growth in the very early stages of a disc's life.

Dust grains limited in size by fragmentation tend to become smaller with time, except during the formation phase of the disc. This is because the fragmentation limit depends linearly on the gas surface density, which decreases over time. Since the dust growth timescale is much shorter than the lifetime of the disc (Eq. 1.33), dust grains limited in size by fragmentation are largest towards the end of the disc formation phase when gas surface densities are highest, and then become smaller over time.

The evolution of the dust surface density in a model with $v_{\rm f} = 1$ m/s, and $\alpha_{\rm t} = 10^{-4}$ is shown in figure 1.5. With these conditions, the particle size is limited by fragmentation. The dust drains at a similar rate across the disc, leading to a similar disc structure as the disc ages.

1.6 Protoplanetary disc temperature

The temperature in a protoplanetary disc is set by the balance of heating and cooling mechanisms. There are two main processes responsible for heating a protoplanetary disc. The foremost of these is the absorption of stellar radiation, and the second is viscous heating as a result of the release of heat from friction forces between neighboring annuli of gas. Stellar radiation dominates disc heating except at radii $\lesssim$1 au. A disc whose temperature is set by radiation is hotter at the surface and cooler at the midplane where less radiation is able to reach. Viscous heating is most efficient in the midplane of the disc. Therefore, regions dominated by viscous heating are hottest in the midplane and cooler at the surface.

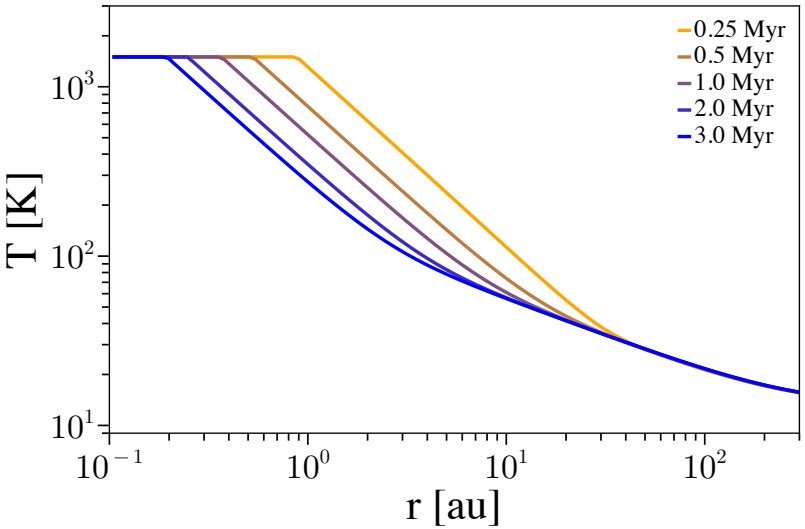

Figure 1.6: Evolution of the disc temperature in a disc heated by stellar irradiation and viscous heating. The temperature in the inner disc does not exceed 1500 K because at that point nearly all elements that make up the dust will have sublimated. The lack of dust reduces the opacity of the disc significantly and makes further heating difficult unless gas opacity is sufficient to heat the disc further.

The temperature of a protoplanetary disc as set by stellar irradiation is given by (e.g. Menou & Goodman, 2004; Kimura et al., 2016)

$$\sigma_{\mathrm{SB}} T_{\mathrm{irr},\star}^4 = \frac{L_\star}{4\pi r^2} \frac{H}{r} \left(\frac{\mathrm{d} \ln H}{\mathrm{d} \ln r} - 1 \right), \tag{1.34}$$

where σ_{SB} is the Stefan-Boltzmann constant and $L_\star$ is the stellar luminosity. The $\mathrm{d} \ln H / \mathrm{d} \ln r$ term is a source of numerical instabilities and is therefore fixed to $9/7$ (Hueso & Guillot, 2005). Combined with the heating due to the ambient background temperature of the cloud core, T_{amb}, the heating rate by irradiation is given by (Menou & Goodman, 2004)

$$\Gamma_{\mathrm{irr}} = \frac{8\sigma_{\mathrm{SB}} \left(T_{\mathrm{irr},\star}^4 + T_{\mathrm{amb}}^4 \right)}{4\left(\tau/2 + 1/\sqrt{3} + 1/\left(3\tau\right) \right)}, \tag{1.35}$$

where τ is the optical depth.

The rate of heating from viscosity is given by (Menou & Goodman, 2004)

$$\Gamma_{\text{Visc}} = \frac{9}{4}\nu\Sigma_{\text{g}}\Omega_{\text{K}}^2. \tag{1.36}$$

Disc cooling occurs primarily by radiative cooling. The rate of cooling due to the disc radiating is described by (Menou & Goodman, 2004)

$$\Lambda_{\text{rad}} = \frac{8\sigma_{\text{SB}}T_{\text{mid}}^4}{3\left(\tau/2 + 1/\sqrt{3} + 1/(3\tau)\right)}. \tag{1.37}$$

The midplane temperatures due to the individual contributions of radiation and viscosity can then be found by setting $\Gamma_{\text{irr}} = \Lambda_{\text{rad}}$ and $\Gamma_{\text{visc}} = \Lambda_{\text{rad}}$. The disc midplane temperature can then be estimated from

$$T_{\text{mid}} = \left(T_{\text{visc}}^4 + T_{\text{irr}}^4\right)^{1/4}. \tag{1.38}$$

The opacity, κ, of the disc is primarily determined by the presence of small dust grains. In this work, we only trace the largest populations of dust grains, and therefore, we do not directly model the disc opacity. However, it has been well established that the dust opacity scales with the disc temperature (e.g. Bell & Lin, 1994). We therefore scale the opacity as $\kappa = 0.0528445T_{\text{mid}}^{0.738}$ (Zhu et al., 2009). The optical depth of the disc is then given by $\tau = \kappa\Sigma_{\text{g}}/2$. In a more detailed model, the scaling law would change as certain elements reach their sublimation temperatures, but the scaling law we use is appropriate in all but the hottest regions of the disc (see Figure 9 of Zhu et al., 2009).

The temporal evolution of the temperature of a disc heated by stellar irradiation and viscous heating, using the same model as in Figure 1.3, is shown in Figure 1.6. The luminosity of the star in this model is scaled as $L = L_{\odot}(M_{\star}/M_{\odot})$ (Baraffe et al., 2002; Liu et al., 2019). The inner disc is efficiently heated by viscous heating, especially during the early stages of disc evolution gas accretion rates are $\gtrsim 10^{-6}\,M_{\odot}$/yr. In the innermost parts of the disc, the temperature does not exceed 1500 K because at that point all solids have sublimated. The loss of opacity from dust prevents further heating unless much lower gas opacity is enough to drive further heating.

1.7 Disc dispersal

A possible physical mechanism for disc dispersal is thermal winds, called photoevaporative winds. These winds are caused by high-energy stellar radiation, typically X-rays, far ultraviolet (FUV), or extreme ultraviolet (EUV), from a stellar source. As this radiation reaches the upper layers of the disc, it can heat the gas to the point where the kinetic energy of a gas molecule exceeds the gravitational binding energy of said molecule. The gas molecule will then be ejected into interstellar space. Photoevaporation can be driven both internally by the star that the disc surrounds (Pascucci et al., 2023), or by external radiation from nearby OB stars (Winter & Haworth, 2022). The work in this thesis concerns low-mass star-forming regions where OB stars are unlikely to form, and hence external photoevaporation is not considered.

The dashed lines in Figure 1.3 show the evolution of a disc undergoing viscous evolution and X-ray photoevaporation, with a photoevaporation model from (Picogna et al., 2021). Prescriptions, like the one used here, for implementing photoevaporation in one-dimensional models of protoplanetary disc evolution are made by fitting a function to mass loss rates found in more advanced three-dimensional simulations of the thermal structure of gas discs. In general, the fitted functions are complicated and not necessary to be reproduced here. I refer to the papers referenced here for their form. In contrast to the disc with pure viscous evolution, the photoevaporative disc is drained of gas faster, and at around 2 Myr it opens up a gap at a distance of $\sim$5 au. The disc inside the gap is cleared of gas within 10^5 yr, and the gap expands outwards, reaching almost 200 au by the time the disc is 3 Myr old.

As shown in Figure 1.3, photoevaporation can efficiently disperse the gas disc on a timescale that is much shorter than that of viscous evolution. However, several uncertainties about the efficiency of photoevaporation exist. The strength of X-ray photoevaporation has been found to be strongly dependent on the frequency of X-rays used, and may depend on the cooling effects included in the model (Sellek et al., 2022). Soft X-rays are able to drive photoevaporative wind more efficiently than hard X-rays. Further, models where photoevaporation is driven primarily by FUV radiation produce significantly lower mass loss rates, and subsequently much longer gas disc lifetimes (Komaki et al., 2021). Heating from FUV radiation is driven by photoelectric heating on small dust grains. The rate of photoevaporation due to FUV radiation is therefore affected by dust evolution (Gorti et al., 2015).

Chapter 2

Observational constraints

In the last decade, the wealth of observational data on protoplanetary discs has increased enormously both in terms of quality and quantity, through the commissioning of the Atacama Large Millimeter/submillimeter Array (ALMA). This has allowed for a much better comparison of protoplanetary disc models and observations, which is rapidly improving our understanding of protoplanetary discs and how they evolve. In this chapter I will give a brief overview of the observational constraints that we have on protoplanetary discs. I will cover measurements of disc masses, the sizes of dust grains, disc lifetimes, disc structures and how disc properties depend on the stellar mass.

2.1 Disc masses

Dust masses

Dust disc masses are estimated from the disc flux at cm/mm wavelength. Surveys of star-forming regions have revealed that dust discs are initially very massive. Median dust disc masses of class 0 and I objects in the Perseus star-forming region are 148 and 52 Earth masses, respectively (Tychoniec et al., 2020), with some class 0 objects having dust masses in excess of 1000 Earth masses. Over a timescale of a few million years, the typical dust disc mass decreases by one or two orders of magnitude. By the class II phase, typical dust disc masses are $\sim$1 Earth mass to $\sim$10 Earth masses (Ansdell et al., 2016; Bai et al., 2016; Ruíz-Rodríguez et al., 2018; Williams et al., 2019; Cazzoletti et al., 2019; Grant et al., 2021; Villenave et al., 2021). A cumulative distribution of dust masses of class 0, I, and II discs is

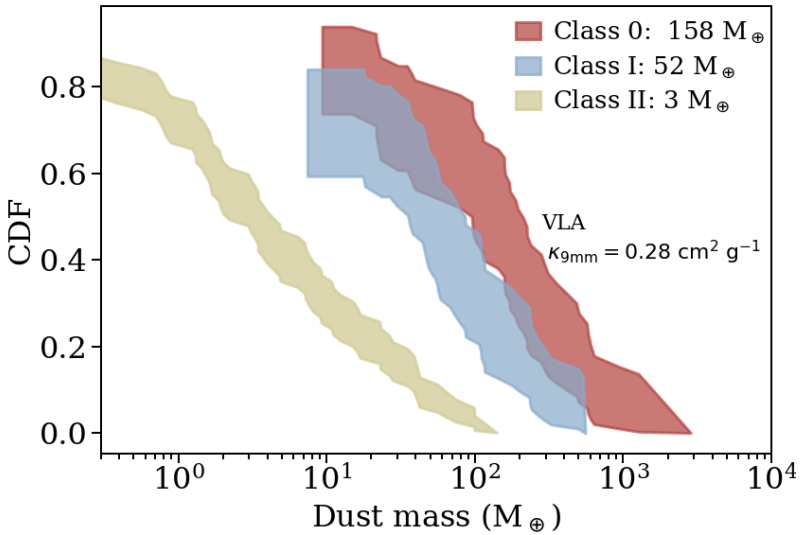

Figure 2.1: Cumulative distribution of disc masses in class 0, I, and II objects. Discs are initially very massive with typical dust masses $> 100\,M_\oplus$. As the discs evolve, this decreases to $\sim$50 $M_\oplus$ by the class I stage and $\sim$3 $M_\oplus$ by the class II stage. Credit: Tychoniec et al. (2020), reproduced with permission from ©ESO.

shown in Figure 2.1.

Estimates of dust disc masses are often made by assuming that the disc emission is optically thin. Under such conditions, estimating the dust mass is relatively straightforward. From the disc flux, it can be calculated as

$$M_{\mathrm{Dust}} = \frac{F_\nu d^2}{\kappa_\nu B\left(T\right)}, \tag{2.1}$$

where F_ν is the observed flux, d is the distance to the object, κ_ν is the opacity of the disc at the observing wavelength, T is the disc temperature, and B is the Planck function (Hildebrand, 1983). With the advent of ESA's space telescope Gaia, distances are known with great accuracy for nearby star-forming regions (Gaia Collaboration et al., 2016). The true opacity and temperature of the disc will vary across the disc. However, to use Eq. (2.1), a representative value for the whole disc must be found. The opacity is chosen based on dust opacity models, but these models do not necessarily produce consistent results across particle size and observing wavelength (e.g., Woitke et al., 2016; Bitsch et al., 2018). The

representative temperature is chosen from SED modeling of protoplanetary discs (Andrews & Williams, 2005), typically to be 20 K, but this is sometimes scaled with the stellar luminosity as $T \propto L_{\star}^{0.25}$ (Andrews et al., 2013; Pascucci et al., 2016).

The possible discrepancies between the assumed representative values of the opacity and temperature make the dust mass estimate less accurate. However, the more major concern with using Eq. (2.1) to estimate dust masses is that protoplanetary discs may not be optically thin. A large amount of dust may therefore be hidden underneath the optically thick surface. To an extent, this can be overcome by observing at longer wavelengths where the emission is more optically thin (e.g., Tobin et al., 2018; Tychoniec et al., 2018, 2020). Several studies have investigated the possible underestimation of dust masses using Eq. (2.1). By modelling the dust emission from observed protoplanetary discs, such studies have revealed that dust masses may be underestimated by a factor of up to 6 (e.g., Ballering & Eisner, 2019; Ribas et al., 2020; Macías et al., 2021). In extreme cases of radially small but very massive discs, the dust mass estimate from Eq. (2.1) could underestimate the true dust mass by up to two orders of magnitude (Liu et al., 2022).

Gas masses

Estimating the gas masses in protoplanetary discs is significantly more difficult than estimating the dust masses. The fundamental problem is that the vast majority of the gas mass is present in molecular hydrogen, which has no significant emission at the typical temperatures found in protoplanetary discs. Therefore, other methods of probing the gas mass have been developed. One is to trace another species of gas that does have significant emission, e.g., carbon monoxide or hydrogen deuteride, and convert this to a hydrogen mass according to an abundance ratio, which I expand on below (Bergin et al., 2013; Kama et al., 2016; Trapman et al., 2017; Booth et al., 2019; Booth & Owen, 2020). A second method is to convert dust masses into gas masses, assuming that the dust mass is 1 % of the gas mass, as is typical of the interstellar medium (e.g., Manara et al., 2016), and thus thought to be representative of the initial conditions of protoplanetary discs.

Both of the methods above suffer from problems. The abundance ratios of H_2 to other gas species are usually highly uncertain, resulting in large errors on mass estimates. CO is especially uncertain because it freezes out and can be locked up as ice in solid bodies, which will affect the abundance ratio of gas-phase carbon to hydrogen (Miotello et al., 2023). Isotopologues of CO that are more able to

accurately trace the gas mass also often have weak lines, making large surveys difficult. Although they have been successfully used to determine the gas mass in a few protoplanetary discs (Booth et al., 2019; Booth & Owen, 2020).

Converting dust masses to gas masses suffers from the obvious problem that dust and gas evolution in protoplanetary discs are different. Most significantly, radial drift of pebbles results in the dust disc draining faster than the gas disc. Hence, assuming the initial dust-to-gas ratio of the disc was 0.01, estimating the gas mass from this only provides a lower limit on the mass.

The large uncertainties in measured gas masses unfortunately make a comparison with disc models difficult, which is part of the reason why the focus in this thesis lies on the dust masses.

2.2 Dust particle sizes

The size of dust particles has been constrained in two main ways. The first and most common method is to use the properties of the disc opacity. If dust emission is optically thin, and the opacity is dominated by absorption, and emissions are in the Rayleigh-Jeans limit, there exists a relation between the slope of the SED and the slope of the dust absorption coefficient

$$I_\nu \propto \nu^{2+\beta} \Rightarrow 2 + \beta = \frac{\mathrm{d} \ln I_\nu}{\mathrm{d} \ln \nu}, \tag{2.2}$$

where I_ν is the intensity of light emitted at the frequency ν, and β is the opacity index. A maximum particle size can then be inferred using a relationship between β and the dust size distribution. Measurements of the opacity index of class II discs have found that it is low, between 0-1 (e.g., Ricci et al., 2010; Ansdell et al., 2018; Tazzari et al., 2021b). An opacity index this low can be explained if the largest particles are mm-cm in size (Pollack et al., 1994). The spectral index, which under the above-mentioned conditions is given by $\alpha = 2 + \beta$, has been found to be radially increasing (Carrasco-González et al., 2019; Macías et al., 2021; Tazzari et al., 2021a), which can be explained by a radially decreasing maximum particle size. The radial size distribution of the maximum particle size in the disc HL Tau is shown in Figure 2.2. In this disc, the particle size ranges from 1.4 mm in the innermost disc to 0.6 mm at 100 au.

The second method of estimating dust sizes is to use the properties of polarized light from protoplanetary discs. These estimates are based on the principle that polarization induced by scattering is only seen if $a \approx \lambda/2\pi$, where a is the particle

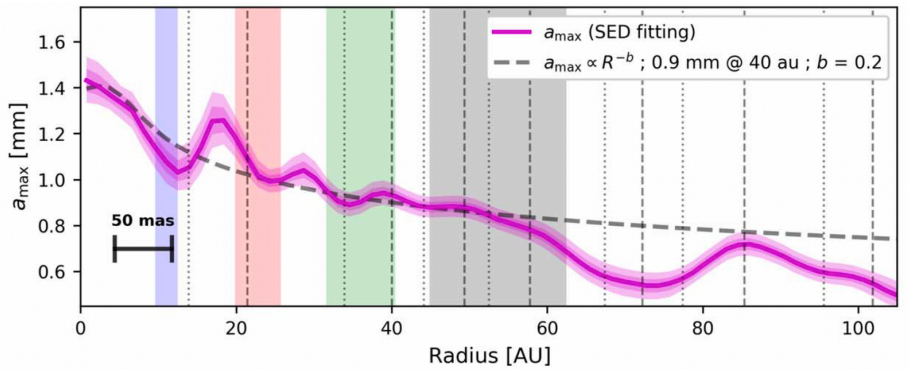

Figure 2.2: Radial distribution of the maximum particle size in HL Tau. Particle sizes range from down to $\sim$0.5 mm in the outer regions of the disc to $\gtrsim$1 mm in the innermost disc. Credit: Carrasco-González et al. (2019), reproduced with permission from ©AAS.

size and λ the observing wavelength (Kataoka et al., 2015). Such polarized light has been observed in several protoplanetary discs at a wavelength of $\sim$1 mm, but not at longer wavelengths. This indicates that the maximum particle size is on the order of 100 μm (Kataoka et al., 2016a,b, 2017; Hull et al., 2018; Dent et al., 2019).

There are a number of proposed solutions to the discrepancy in dust particle sizes derived from the spectral index and from polarization. A low spectral index can be achieved not only by particle growth but also through discs being optically thick but with small dust grains (Ricci et al., 2012). On the other hand, mm-sized grains that are very settled to the disc midplane, due to very low disc turbulence, can explain the polarized disc emission (Ueda et al., 2021). Emission from non-spherical dust grains is also more polarized than spherical grains, providing another possible pathway to alleviate the tension in dust sizes (Kirchschlager et al., 2019).

2.3 Disc sizes

The physical size of a protoplanetary disc is difficult to define because the disc will gradually fade into the background of the giant molecular cloud. Pragmatic approaches to defining disc sizes are therefore used. If the mass distribution of the disc is known, as in numerical models, the radius containing a large fraction of the total mass is a simple way to track the radial extent of the disc. When observing

discs, however, only the flux is known. Using this, a common definition of disc size is the flux radius. This is defined as the radius containing a fraction of the total flux, typically 68 % or 95 %, and is determined by fitting a profile to the observed radial intensity profile (Tripathi et al., 2017). This profile can then be integrated to find radius which contains the selected fraction of the total flux. The 68 % radius is less sensitive to the fitting profile used (Sanchis et al., 2020) but may miss weak emission from the outermost regions of the disc.

Surveys of protoplanetary discs have revealed that for class II discs, the 68 % flux radius ranges from a few astronomical units to a few hundred astronomical units (Hendler et al., 2020). In a recent survey of class 0 and I objects, most discs have 95 % flux radii between 4 au to $\sim$60 au, although a few extend to several hundred astronomical units (Ohashi et al., 2023).

As radial drift of pebbles can cause the outer radius of the dust disc to shrink, and a viscously evolving gas expands with time, one might be able to infer the presence of radial drift from a size difference between the dust and gas disc. However, differences in the size of protoplanetary discs can be explained by differences in the optical depth of millimeter continuum emission and CO lines, which are used to trace gas, without the need for radial drift (Facchini et al., 2017). A gas disc that is more than 4 times larger than the dust disc is considered necessary to be a clear sign of radial drift (Trapman et al., 2019). This has been found to be the case in the CX Tauri disc, where the 68% flux radius of the gas is over 5 times larger than the 68% flux radius of the dust (Facchini et al., 2019).

2.4 Disc lifetimes

Estimating the average expected disc lifetime is typically done by measuring the fraction of stars with discs in star-forming regions. The presence of a disc is inferred from an infrared excess originating from the presence of cold dust. Doing this across several star forming regions, and with estimates of the age of the regions, the typical disc lifetime can be estimated by fitting disc fraction as

$$f_{\text{disc}} = Ae^{-t/\tau}, \tag{2.3}$$

where A is the initial disc fraction, t is the age of the cluster, and τ is the expected disc lifetime. The initial disc fraction can be $< 100\%$ since a fraction of stars form as binaries, and this process can disrupt disc formation. Using this method, typical disc lifetimes of 2-3 Myr have been found (e.g. Haisch et al., 2001; Mamajek, 2009; Ribas et al., 2014, 2015). However, this number may be underestimated

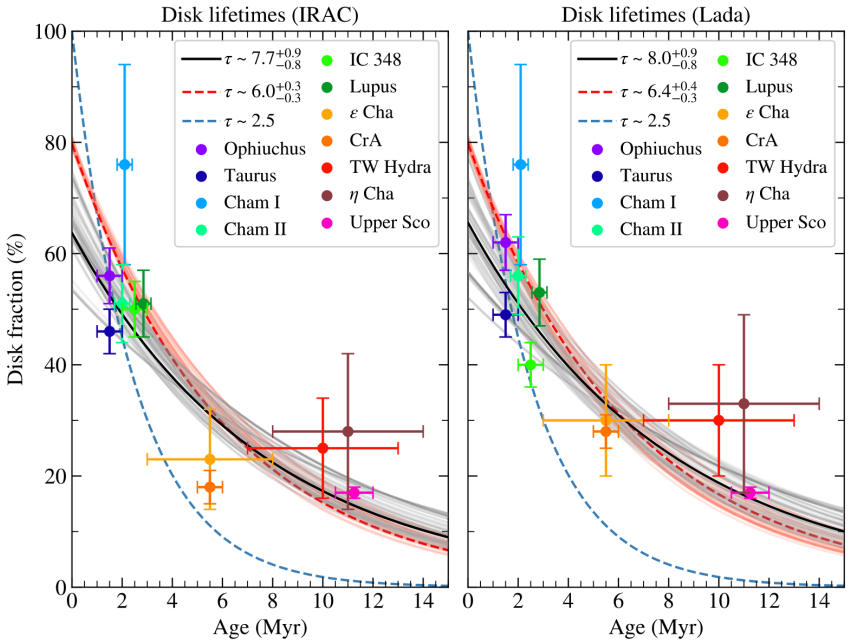

Figure 2.3: Disc fraction as a function of the age of the star forming regions. The right panel shows this whose evolutionary stage has been classified according to the Lada system explained in Section 1.1, and the left panel a classification system based on the infrared slope at Spitzer IRAC wavelengths. Typical disc lifetimes in this sample are 6-8 Myr. Credit: Michel et al. (2021), reproduced with permission from ©AAS.

due to selection effects (Pfalzner et al., 2014). Indeed, more recent estimates using nearby low-mass star-forming regions find disc lifetimes as high as 6-8 Myr (Michel et al., 2021). Figure 2.3 shows the disc fractions and estimated typical disc lifetimes as derived in (Michel et al., 2021).

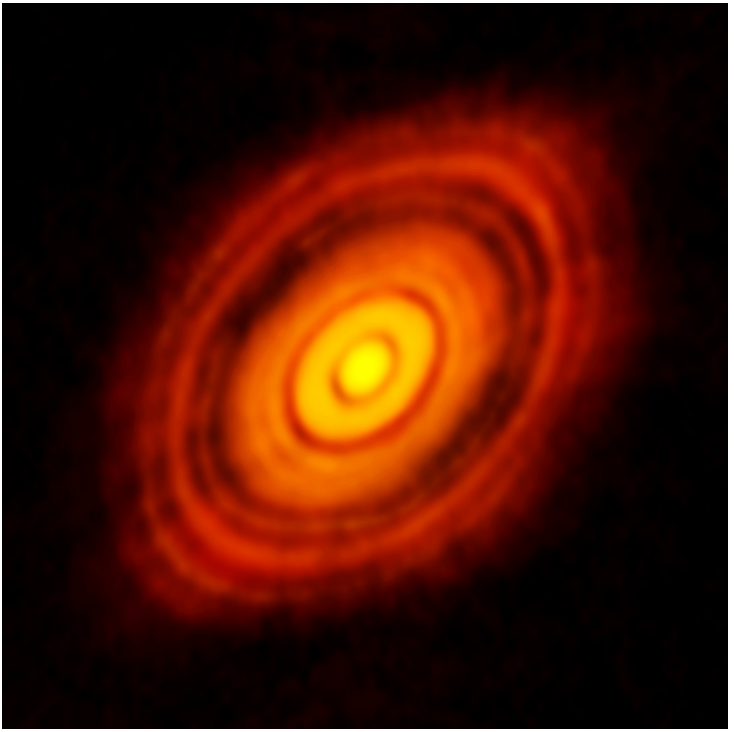

Figure 2.4: The dust component of the protoplanetary disc with ALMA at a wavelength of 1.3 mm. The disc is very structured, showing clear rings and gaps, which could be a signature of ongoing planet formation. Credit: ALMA (ESO/NAOJ/NRAO).

2.5 Disc structures

Detailed high-resolution surveys of protoplanetary dust discs have revealed that many of them display significant structure. Rather than being smooth, they have rings, gaps, and spiral arms (e.g. ALMA Partnership et al., 2015; Andrews et al., 2018). A famous example of a structured disc is HL Tau shown in Figure 2.4. The origin of these structures is not fully understood. Proposed mechanisms include for example ice lines and the cores of giant planets.

Ice lines are able to produce disc structures when the fragmentation limit changes as the particles sublimate at ice lines and the composition of the grains change. This can lead to the formation of gaps and rings (Pinilla et al., 2017). In

the scenario of giant planet formation, once the core of the protoplanet reaches a mass of about 10 $M_{\oplus}$, the so-called pebble isolation mass, it inverts the nearby pressure gradient causing a pressure maximum outside of the orbit of the core (Lambrechts & Johansen, 2014; Bitsch et al., 2018). The lack of a pressure gradient at the maximum means the dust particles experience no gas drag and do not drift. Pressure bumps are thus able to trap pebbles and create rings and gaps in the dust structure.

Structured discs have been found to correlate with the stellar mass, which in turn can be linked to the demographics of giant planets (van der Marel & Mulders, 2021). Due to a limitation in spatial resolution, it remains unclear if compact discs are smooth or structured. However, a recent reanalysis of compact discs in Taurus found structures in 6 out of 12 discs studied (Zhang et al., 2023). Disc structures are also found to be present even in very young discs (Michel et al., 2023).

Dust that is concentrated at the edges of gaps may not be completely trapped there. As large particles collide and fragment into smaller particles, the small particles can diffuse across the gap, if the diffusivity of dust particles is strong enough (Stammler et al., 2023). Gaps that are close to the host star might be unable to trap even mm-sized dust grains (Kalyaan et al., 2023).

2.6 Dependence on stellar mass

Computational studies of the evolution of protoplanetary discs have tended to focus on the evolution of discs around solar-mass stars. Similarly, high-resolution detailed observational surveys of protoplanetary discs are biased towards the biggest and brightest objects. However, from the initial mass function of stars, (e.g. Kroupa, 2001), we know that $\sim$90% of stars are less massive than 0.7 $M_{\odot}$. Sun-like stars are, in fact, quite rare. Therefore, it is important to study how disc properties vary with stellar mass.

The dust mass of protoplanetary discs has been found to correlate with the stellar mass across several star-forming regions as $M_{\rm Dust} \propto M_{\star}^{1.3-1.9}$ (Pascucci et al., 2016; Ansdell et al., 2017), shown in Figure 2.5. One of the discoveries of these surveys is that older star-forming regions have a steeper scaling than younger regions. Pascucci et al. (2016) investigated the cause of the steepening with time and found that dust particles undergoing growth, fragmentation, and radial drift show a behavior consistent with observations. This is because the timescale for radial drift to remove mm-sized particles is shorter around lower-mass stars. More massive stars are, therefore, able to remain bright at mm-wavelengths for longer.

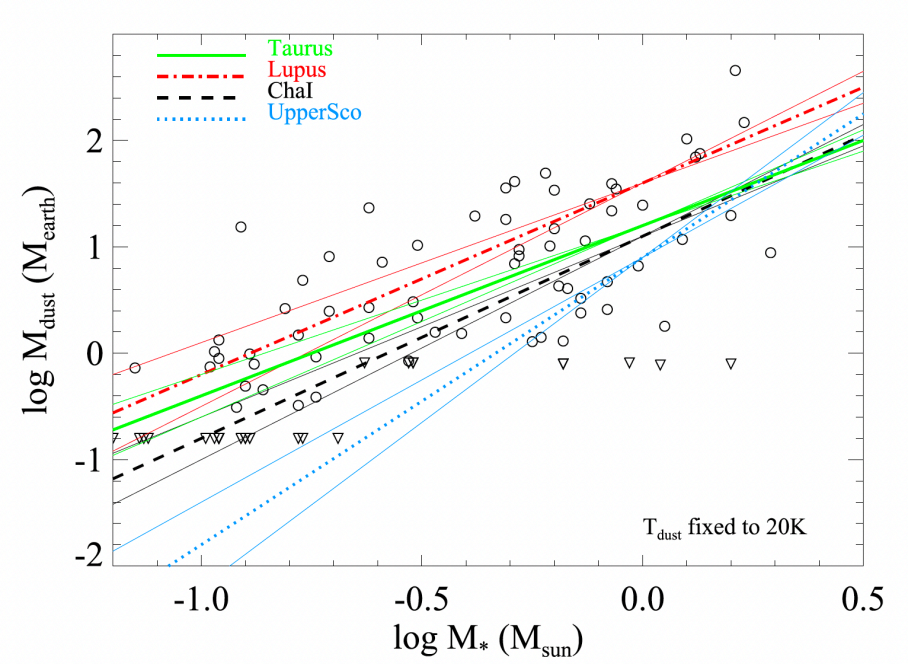

Figure 2.5: Dust mass as a function of stellar mass in star-forming regions. The slope of the scaling ranges from 1.3 to 1.9. The older region Upper Scorpius has the steepest scaling, suggesting that this relation becomes steeper as the star forming regions ages. Credit: Pascucci et al. (2016), reproduced with permission from ©AAS.

Pinilla et al. (2020) found that the $M_{\rm Dust} - M_\star$ relation could be reproduced in a disc evolution model if the initial disc mass scales with the stellar mass, and strong pressure traps are present.

It has been known for several decades that the mass accretion rate scales with the stellar mass with a steeper-than-linear relation (e.g. Hillenbrand et al., 1992; Muzerolle et al., 2003; Mohanty et al., 2005; Natta et al., 2006). The slope has typically been found to be 1.6-2; however, the spread in the mass accretion rate is large (e.g. Alcalá et al., 2014, 2017; Manara et al., 2017). The large spread is largely physical in nature and not caused by observational uncertainties (Manara et al., 2023). However, it is not clear if the spread is due to disc evolution or due to variations in the initial conditions of star and disc formation.

Chapter 3

Radial drift in protoplanetary discs

In this chapter I will highlight the most important results from my research, and explain the population synthesis model that was in some way used in each paper. I will then give a brief outlook on the future of the field.

3.1 Population synthesis

As discussed in Section 2.6, several disc properties have shown a dependence on the stellar mass. This could be due to differences in disc evolution timescales around stars of different stellar masses, but it is likely that it is also due to variations in the initial conditions, e.g. the disc mass, across stellar mass. Because the protoplanetary disc model developed in this thesis includes the formation of the star and disc, the initial conditions are those of the molecular cloud core.

The aim when selecting the initial conditions is to start from reasonable values and create a population of discs whose masses are similar to what is observed in very young discs. To achieve this, we chose to vary two parameters of the cloud core as our initial conditions: the mass and angular momentum of the cloud core. While the temperature could also be varied, we opted to keep it constant at 10 K across all cloud cores. The size of a Bonnor-Ebert sphere scales linearly with the temperature. Therefore, the effect of increasing the temperature is to make the collapse of the cloud core take a longer time (see Equation 1.13).

To achieve a realistic range of masses, we selected the masses from the stellar initial mass function (IMF) of Kroupa (2001). In detail, the IMF of stars might differ from the core mass function (CMF) of molecular cloud cores. However, functionally, they are alike with similar slopes and exhibiting a rapid reduction in

the occurrence rate at high masses (McKee & Ostriker, 2007).

We set the angular momentum by choosing the centrifugal radius. The ratio of the rotational energy to the gravitational energy has no clear dependence on the size of molecular cloud cores (Chen & Ostriker, 2018). As shown in Paper I, if one assumes this ratio to be independent of the mass of the cloud core, the centrifugal radius scales linearly with the stellar mass. Therefore, we scale the centrifugal radius as

$$R_{\rm C} = R_1 \left(\frac{M_{\rm core}}{M_\odot} \right), \tag{3.1}$$

where $M_{\rm core}$ is the mass of the cloud core. The appropriate value of R_1 is not immediately clear. Numerical studies of star formation have found that magnetic braking can remove angular momentum from the infalling material during the collapse of the cloud core. This phenomenon was first reported by Allen et al. (2003), where under ideal MHD, disc formation was suppressed, and it was dubbed the 'magnetic braking catastrophe'. Further studies have found that non-ideal MHD effects reduce the effectiveness of magnetic braking, but precisely how strong the effect is remains unclear (Wurster et al., 2019; Lee et al., 2021). Due to this uncertainty, the value chosen for R_1 is not consistent across paper I and II, and the effects of this on the resulting disc size was examined in paper III.

In addition to varying the mass and angular momentum of the cloud core, we assigned the discs an internal age spread of 1 million years. That is to say, the oldest disc in our model is assumed to have formed 1 Myr before the youngest disc. This is done to emulate the fact that not all discs will form at the same time. At least in the star forming region Taurus, star formation is thought to have gone on for 1-2 Myr (Kenyon & Hartmann, 1995).

3.2 Evolution of the cumulative distribution of dust masses

In the second paper, we expanded upon the model used in the first paper to include the growth of dust and limiting it in size by fragmentation and drift. In addition to this, we also calculate the disc temperature from stellar irradiation and viscous heating. Disc dispersal was included by way of one of two photoevaporation models. These were the strongly evaporating X-ray model of Picogna et al. (2021) and the weakly evaporating FUV model of Komaki et al. (2021). We included both of these as there is not yet a consensus on the strength of photoevaporation, and these two models cover the ends of plausible photoevaporation rates. We used

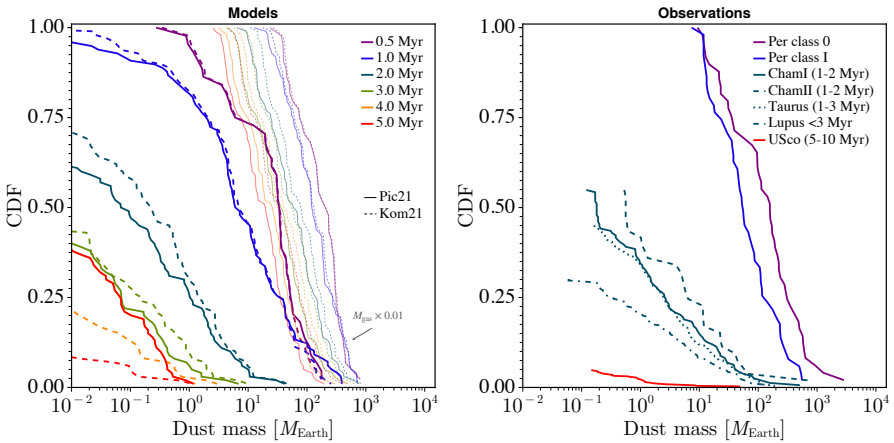

Figure 3.1: Cumulative distributions of dust disc masses. The left panel shows a population synthesis model. The thick lines show the model undergoing radial drift and the thin lines a model where the dust only advects with the gas. The right panel shows the distribution of dust disc masses in a few star-forming regions. Credit: Appelgren et al. (2023).

the expanded protoplanetary disc model to run a population synthesis model as explained in Section 1.

The main aim of the paper was to compare the temporal evolution of the cumulative distribution of dust disc masses to a sample of real observed discs, whose mass has been determined assuming optically thin emission, as described in Chapter 2, Section 1.

Figure 3.1 shows the evolution of the cumulative dust mass distribution for discs evolving under $\alpha_\nu = 10^{-2}$, and both of the photoevaporation models (left panel). The thick lines show a model with radial drift, and the thin lines show a model without radial drift, where the dust only traces the gas. The right panel shows a sample of protoplanetary discs from both class 0, I, and II objects. The discs with radial drift are able to reproduce the observed depletion trend quite well. The discs without radial drift are unable to match this depletion. They only agree with the observed sample of class 0/I discs, which is reasonable as in these discs radial drift will not have had as much time to affect the dust mass evolution. The solid and dashed lines show the X-ray photoevaporation model and FUV photoevaporation model, respectively. The X-ray model opens a gap in the gas disc earlier, allowing for more discs to retain some dust outside the gap. However,

at most $\sim 3\,M_\oplus$ of dust is retained.

One place where the model and observations differ is that in the observed sample of discs there exists a population of older discs with high dust masses ($\gtrsim 100\,M_\oplus$). This group of discs is absent in the model. We speculate that this represents a population of discs whose dust mass evolution is not dominated by radial drift. Instead, these discs have significant structures, originating from the cores of giant planets, where pebbles are trapped, or at the very least, slowed down. These discs are proposed to make up 5 %-15 % of the total disc population. Structured discs are found to be more common around high-mass stars, which in turn also host more giant planets (van der Marel & Mulders, 2021). The reduction in the dust mass of these discs might instead be dominated by trapped pebbles growing to large sizes and reducing their mm-emission (Pinilla et al., 2020).

3.3 Evolution of the disc sizes

In Paper III, we studied how the relationship between the mm-flux from the dust disc and the flux radius evolves over time. We explored how the flux and disc size depend on the angular momentum of the disc and on the efficiency of viscous heating in the disc.

A higher angular momentum of the molecular cloud core results in both material landing further from the protostar during the infall phase and more material landing on the disc rather than directly onto the protostar. More angular momentum thus leads to a bigger and more massive disc. If the disc is optically thin and observed face-on, the intensity emitted from the disc can be approximated as

$$I_\nu = B_\nu \Sigma_\mathrm{d} \kappa_\nu. \tag{3.2}$$

Therefore, in this limit, a more massive disc leads to a higher disc flux.

The total flux also depends on the disc temperature, and therefore stronger viscous heating leads to higher fluxes. Because viscous heating is efficient only in the inner disc, it affects the radial temperature structure of the disc and therefore also the flux radius. A disc with weak viscous heating will result in larger flux radii as the total emission is less concentrated to the inner disc.

We ran a protoplanetary disc model including disc formation, viscous evolution of the gas, and growth and radial drift of the dust component. We assumed a viscous alpha of $\alpha_\nu = 10^{-2}$, a fragmentation velocity of $v_\mathrm{f} = 1\,\mathrm{m/s}$, and a turbulent stirring alpha of $\alpha_\mathrm{t} = 10^{-4}$. To investigate discs with less efficient viscous heating, we set $\alpha = 10^{-3}$ for calculating the viscous heating, keeping it as a separate parameter from α_ν.

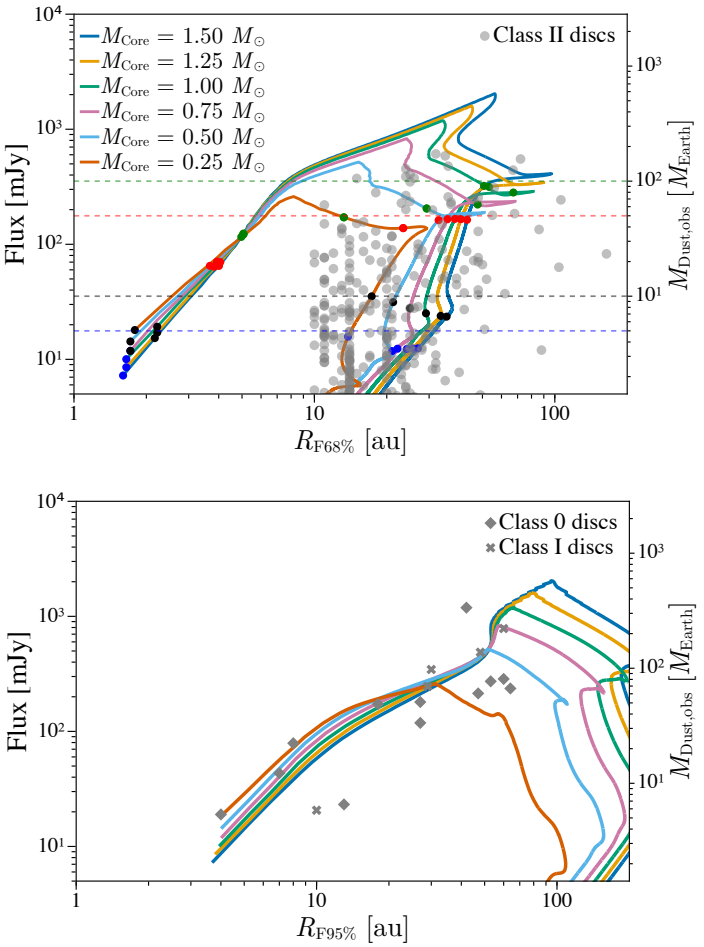

Figure 3.2: Total flux at a wavelength of 1.3 mm as a function of the radius containing 68% (left panel) and 95% (right panel) of said flux. Discs start out on the left branch, and the flux and size increase as the disc forms. Once the formation phase is over, the flux begins to decrease as the disc mass decreases and the disc is less viscously heated. The apparent size of the disc continues to increase for a while as the inner disc become cooler, and because small dust in the outer disc advects outwards with the gas. Eventually, radial drift of pebbles becomes efficient and the size of the disc also begins to decrease.

For this project, we calculate the flux radius of the modeled discs by directly integrating the intensity profile emitted from the discs. This method differs in detail from that used for observations of real discs, which requires fitting a profile to the observed radial intensity profile and integrating the fitted profile. For a more accurate comparison, a similar method could be applied to the modeled discs as well. However, assuming that the fitted profile accurately traces the true profile, the methods we use should be sufficient. The 68% radius is not very sensitive to the chosen profile, suggesting that sizes are accurately traced, but the 95% radius is more sensitive.

We evolved a set of discs created from cloud cores with masses from 0.25 $M_\odot$ to 1.5 $M_\odot$, tracing how they evolve in flux as a function of flux radius, shown in Figure 3.2 on the following page. The evolution can in this plane be divided into three phases. As the disc is forming, the equivalent of the class 0/I stage, both the flux and the size increase. This is the left branch in Figure 3.2. After this, there is a phase where the flux decreases whilst the flux radius continues to increase. This increase is both due to a decrease in viscous heating due to the removal of gas from the disc and due to a physical expansion of the dust disc from dust particles advecting outwards with the expanding gas disc. Finally, there is a phase corresponding to when disc evolution is dominated by radial drift. This is represented in the right branch where both the flux and disc radius decrease.

The discs shown in Figure 3.2 are evolved under less efficient viscous heating and a high angular momentum budget. We scaled the centrifugal radius as $R_\mathrm{C} = 40\,(M_\mathrm{core}/M_\odot)$ au, where M_core is the mass of the cloud core. The background markers in Figure 3.2 show observed class II discs in the left panel and class 0/I discs in the right panel. The class II discs are taken from Pascucci et al. (2016); Andrews et al. (2018); Ansdell et al. (2018); Cieza et al. (2019); Akeson et al. (2019); van der Marel & Mulders (2021), and the class 0/I discs from Ohashi et al. (2023). The best agreement with the class 0/I discs was found with this scaling of the centrifugal radius and weak viscous heating. Less angular momentum and stronger viscous heating lead to discs that are too small compared to the class 0/I objects. We also show that it is the combination of higher angular momentum and weaker viscous heating that is necessary, as the contribution of each on its own is not enough.

Viscous heating has been inferred in a number of observed protoplanetary discs using various methods. The most robust detection of viscous heating is through absorption lines in the disc. Absorption lines signify viscously heated discs because accretion heating can result in a midplane temperature higher than

that of the disc surface. This has been observed in discs around massive stars (Barr et al., 2022), although not in discs around T-Tauri stars (Carr & Najita, 2011). Viscous heating has also been inferred in the IRS 7B-a disc from the eDisk sample of class 0/I discs that we compare our model to (Takakuwa et al., 2024). Through modeling of the 1.3 mm continuum emission, the authors found that viscous heating at an accretion rate of $\sim 10^{-6}$, $M_{\odot}$/yr was necessary to reproduce the observed intensity of IRS 7B-a. Modelling of the thermal structure of FU Orionis-type stars have also found viscous heating to be necessary to explain observed fluxes (Labdon et al., 2021; Alarcón et al., 2023).

The calculation of fluxes, as shown in Figure 3.2, was done using the midplane temperature of the disc. In the case of an isothermal disc, as is the case if the disc is optically thin, this is the same as the surface temperature of the disc. However, for an optically thick disc that is viscously heated, the surface temperature, i.e., the temperature that is observed, is lower than the midplane temperature. The discs in our model are generally optically thick at a wavelength of 1.3 mm during the formation of the discs. The surface temperature of an optically thick disc that is viscously heated scales as $T_{\rm surf} \propto T_{\rm mid}(\tau)^{-1/4}$. Therefore, the fluxes from our model discs during their formation is likely somewhat overestimated. Additionally, the flux from the model discs was calculated as the face-on flux. The observed disc are, however, inclined with respect to the observer, which, due to geometrical effects, is likely to be at around 70°. Unless the discs are completely optically thin in every direction, the flux of an inclined disc will be smaller than that of a face-on disc. Hence, the true fluxes of the observed sample might be higher than given here.

Summary

From the result presented here, the evolution of the dust mass in protoplanetary discs through radial drift appears consistent with the majority of observed discs. Discs without radial drift are unable to reproduce the observed change in the cumulative distribution of dust masses over time. The evolution of the mm-flux as a function of the flux radius in discs undergoing viscous evolution and radial drift of dust is also able to cover a range or radii and fluxes similar to that observed in real protoplanetary discs.

Future outlook

In the near future, our observational understanding of both protoplanetary discs will continue to improve from continued surveys with ALMA. With the start of operations of the James Webb Space Telescope (JWST), our understanding of protoplanetary disc chemistry is set to increase rapidly. Drifting icy pebbles can enhance the local abundance of water vapour as the sublimate at the water snow line (Kalyaan et al., 2021, 2023). This effect has been detected with JWST and interpreted as a sign of efficient radial drift (Banzatti et al., 2023).

Our inventory of known exoplanets is also set to increase significantly. The Transiting Exoplanet Survey Satellite (TESS), launched in 2018, has found several hundred confirmed exoplanets, and many thousands more candidates waiting to be confirmed. The Gaia telescope is expected to detect thousand or even tens of thousands of exoplanets (Sozzetti et al., 2014; Perryman et al., 2014; Holl et al., 2023). Two exoplanets have already been discovered by Gaia, although using the transit method rather than astrometry (Panahi et al., 2022). A better understanding of both protoplanetary discs and exoplanets will hopefully allow us to better connect the two populations and, in turn, further our understanding of planet formation.

The transition towards protoplanetary disc models with magnetic wind-driven accretion, and thus more realistic disc evolution, is set to accelerate. In recent years, much effort has been put into developing wind-driven disc models that are similarly user-friendly as the classical α-disc model (Bai, 2016; Suzuki et al., 2016; Tabone et al., 2022a). Such models have been shown to be able to reproduce the observed correlation between the accretion rate and disc mass (Tabone et al., 2022b).

With an ever increasing catalogue of exoplanets and well studied protoplanetary discs, in addition to significant advances in the theory of protoplanetary disc evolution and planet formation over the past decade, the future looks bright.

References

Akeson, R. L., Jensen, E. L. N., Carpenter, J., et al. 2019, ApJ, 872, 158, doi: 10.3847/1538-4357/aaff6a

Alarcón, F., Casassus, S., lyra, W., Pérez, S., & Cieza, L. 2023, arXiv e-prints, arXiv:2311.17195, doi: 10.48550/arXiv.2311.17195

Alcalá, J. M., Natta, A., Manara, C. F., et al. 2014, A&A, 561, A2, doi: 10.1051/0004-6361/201322254

Alcalá, J. M., Manara, C. F., Natta, A., et al. 2017, A&A, 600, A20, doi: 10.1051/0004-6361/201629929

Allen, A., Li, Z.-Y., & Shu, F. H. 2003, ApJ, 599, 363, doi: 10.1086/379243

ALMA Partnership, Brogan, C. L., Pérez, L. M., et al. 2015, ApJL, 808, L3, doi: 10.1088/2041-8205/808/1/L3

Alves, J. F., Lada, C. J., & Lada, E. A. 2001, Nature, 409, 159

Andrews, S. M., Rosenfeld, K. A., Kraus, A. L., & Wilner, D. J. 2013, ApJ, 771, 129, doi: 10.1088/0004-637X/771/2/129

Andrews, S. M., & Williams, J. P. 2005, ApJ, 631, 1134, doi: 10.1086/432712

Andrews, S. M., Huang, J., Pérez, L. M., et al. 2018, ApJL, 869, L41, doi: 10.3847/2041-8213/aaf741

Ansdell, M., Williams, J. P., Manara, C. F., et al. 2017, AJ, 153, 240, doi: 10.3847/1538-3881/aa69c0

Ansdell, M., Williams, J. P., van der Marel, N., et al. 2016, ApJ, 828, 46, doi: 10.3847/0004-637X/828/1/46

Ansdell, M., Williams, J. P., Trapman, L., et al. 2018, ApJ, 859, 21, doi: 10.3847/1538-4357/aab890

Appelgren, J., Lambrechts, M., & Johansen, A. 2020, A&A, 638, A156, doi: 10.1051/0004-6361/202037650

Appelgren, J., Lambrechts, M., & van der Marel, N. 2023, A&A, 673, A139, doi: 10.1051/0004-6361/202245252

Bai, X.-N. 2013, ApJ, 772, 96, doi: 10.1088/0004-637X/772/2/96

—. 2016, ApJ, 821, 80, doi: 10.3847/0004-637X/821/2/80

—. 2017, ApJ, 845, 75, doi: 10.3847/1538-4357/aa7dda

Bai, X.-N., & Stone, J. M. 2013, ApJ, 769, 76, doi: 10.1088/0004-637X/769/1/76

Bai, X.-N., Ye, J., Goodman, J., & Yuan, F. 2016, ApJ, 818, 152, doi: 10.3847/0004-637X/818/2/152

Balbus, S. A., & Hawley, J. F. 1991, ApJ, 376, 214, doi: 10.1086/170270

Ballering, N. P., & Eisner, J. A. 2019, AJ, 157, 144, doi: 10.3847/1538-3881/ab0a56

Banzatti, A., Pontoppidan, K. M., Carr, J. S., et al. 2023, ApJL, 957, L22, doi: 10.3847/2041-8213/acf5ec

Baraffe, I., Chabrier, G., Allard, F., & Hauschildt, P. H. 2002, A&A, 382, 563, doi: 10.1051/0004-6361:20011638

Barr, A. G., Boogert, A., Li, J., et al. 2022, ApJ, 935, 165, doi: 10.3847/1538-4357/ac74b8

Batygin, K., & Morbidelli, A. 2023, Nature Astronomy, 7, 330, doi: 10.1038/s41550-022-01850-5

Bell, K. R., & Lin, D. N. C. 1994, ApJ, 427, 987, doi: 10.1086/174206

Bergin, E. A., Cleeves, L. I., Gorti, U., et al. 2013, Nature, 493, 644, doi: 10.1038/nature11805

Birnstiel, T., Klahr, H., & Ercolano, B. 2012, A&A, 539, A148, doi: 10.1051/0004-6361/201118136

Bitsch, B., Morbidelli, A., Johansen, A., et al. 2018, A&A, 612, A30, doi: 10.1051/0004-6361/201731931

Blum, J., & Münch, M. 1993, Icarus, 106, 151, doi: 10.1006/icar.1993.1163

Blum, J., & Wurm, G. 2008, ARA&A, 46, 21, doi: 10.1146/annurev.astro.46.060407.145152

Bonnor, W. B. 1956, MNRAS, 116, 351, doi: 10.1093/mnras/116.3.351

Booth, A. S., Walsh, C., Ilee, J. D., et al. 2019, ApJL, 882, L31, doi: 10.3847/2041-8213/ab3645

Booth, R. A., & Owen, J. E. 2020, MNRAS, 493, 5079, doi: 10.1093/mnras/staa578

Burkert, A., & Alves, J. 2009, ApJ, 695, 1308, doi: 10.1088/0004-637X/695/2/1308

Carr, J. S., & Najita, J. R. 2011, ApJ, 733, 102, doi: 10.1088/0004-637X/733/2/102

Carrasco-González, C., Sierra, A., Flock, M., et al. 2019, ApJ, 883, 71, doi: 10.3847/1538-4357/ab3d33

Cazzoletti, P., Manara, C. F., Liu, H. B., et al. 2019, A&A, 626, A11, doi: 10.1051/0004-6361/201935273

Chen, C.-Y., & Ostriker, E. C. 2018, ApJ, 865, 34, doi: 10.3847/1538-4357/aad905

Cieza, L. A., Ruíz-Rodríguez, D., Hales, A., et al. 2019, MNRAS, 482, 698, doi: 10.1093/mnras/sty2653

Dent, W. R. F., Pinte, C., Cortes, P. C., et al. 2019, MNRAS, 482, L29, doi: 10.1093/mnrasl/sly181

Ebert, R. 1957, ZA, 42, 263

Facchini, S., Birnstiel, T., Bruderer, S., & van Dishoeck, E. F. 2017, A&A, 605, A16, doi: 10.1051/0004-6361/201630329

Facchini, S., van Dishoeck, E. F., Manara, C. F., et al. 2019, A&A, 626, L2, doi: 10.1051/0004-6361/201935496

Fischer, D. A., & Valenti, J. 2005, ApJ, 622, 1102, doi: 10.1086/428383

Fulton, B. J., Rosenthal, L. J., Hirsch, L. A., et al. 2021, ApJS, 255, 14, doi: 10.3847/1538-4365/abfcc1

Gaia Collaboration, Prusti, T., de Bruijne, J. H. J., et al. 2016, A&A, 595, A1, doi: 10.1051/0004-6361/201629272

Gorti, U., Hollenbach, D., & Dullemond, C. P. 2015, ApJ, 804, 29, doi: 10.1088/0004-637X/804/1/29

Grant, S. L., Espaillat, C. C., Wendeborn, J., et al. 2021, ApJ, 913, 123, doi: 10.3847/1538-4357/abf432

Greene, T. P., Wilking, B. A., Andre, P., Young, E. T., & Lada, C. J. 1994, ApJ, 434, 614, doi: 10.1086/174763

Gullbring, E., Hartmann, L., Briceño, C., & Calvet, N. 1998, ApJ, 492, 323, doi: 10.1086/305032

Gundlach, B., & Blum, J. 2015, ApJ, 798, 34, doi: 10.1088/0004-637X/798/1/34

Gurrutxaga, N., Johansen, A., Lambrechts, M., & Appelgren, J. 2024, arXiv e-prints, arXiv:2311.04365, doi: 10.48550/arXiv.2311.04365

Haisch, Jr., K. E., Lada, E. A., & Lada, C. J. 2001, ApJL, 553, L153, doi: 10.1086/320685

Hartmann, L., Calvet, N., Gullbring, E., & D'Alessio, P. 1998, ApJ, 495, 385, doi: 10.1086/305277

Hendler, N., Pascucci, I., Pinilla, P., et al. 2020, ApJ, 895, 126, doi: 10.3847/1538-4357/ab70ba

Herczeg, G. J., & Hillenbrand, L. A. 2008, ApJ, 681, 594, doi: 10.1086/586728

Hildebrand, R. H. 1983, QJRAS, 24, 267

Hillenbrand, L. A., Strom, S. E., Vrba, F. J., & Keene, J. 1992, ApJ, 397, 613, doi: 10.1086/171819

Holl, B., Sozzetti, A., Sahlmann, J., et al. 2023, A&A, 674, A10, doi: 10.1051/0004-6361/202244161

Hueso, R., & Guillot, T. 2005, A&A, 442, 703, doi: 10.1051/0004-6361:20041905

Hull, C. L. H., Yang, H., Li, Z.-Y., et al. 2018, ApJ, 860, 82, doi: 10.3847/1538-4357/aabfeb

Ingleby, L., Calvet, N., Herczeg, G., et al. 2013, ApJ, 767, 112, doi: 10.1088/0004-637X/767/2/112

Johansen, A., & Lacerda, P. 2010, MNRAS, 404, 475, doi: 10.1111/j.1365-2966.2010.16309.x

Johansen, A., Ronnet, T., Bizzarro, M., et al. 2021, Science Advances, 7, eabc0444, doi: 10.1126/sciadv.abc0444

Johnson, J. A., Aller, K. M., Howard, A. W., & Crepp, J. R. 2010, PASP, 122, 905, doi: 10.1086/655775

Kalyaan, A., Pinilla, P., Krijt, S., Mulders, G. D., & Banzatti, A. 2021, ApJ, 921, 84, doi: 10.3847/1538-4357/ac1e96

Kalyaan, A., Pinilla, P., Krijt, S., et al. 2023, ApJ, 954, 66, doi: 10.3847/1538-4357/ace535

Kama, M., Bruderer, S., van Dishoeck, E. F., et al. 2016, A&A, 592, A83, doi: 10.1051/0004-6361/201526991

Kandori, R., Nakajima, Y., Tamura, M., et al. 2005, AJ, 130, 2166, doi: 10.1086/444619

Kataoka, A., Muto, T., Momose, M., Tsukagoshi, T., & Dullemond, C. P. 2016a, ApJ, 820, 54, doi: 10.3847/0004-637X/820/1/54

Kataoka, A., Tsukagoshi, T., Pohl, A., et al. 2017, ApJL, 844, L5, doi: 10.3847/2041-8213/aa7e33

Kataoka, A., Muto, T., Momose, M., et al. 2015, ApJ, 809, 78, doi: 10.1088/0004-637X/809/1/78

Kataoka, A., Tsukagoshi, T., Momose, M., et al. 2016b, ApJL, 831, L12, doi: 10.3847/2041-8205/831/2/L12

Kenyon, S. J., & Hartmann, L. 1995, ApJS, 101, 117, doi: 10.1086/192235

Kimura, S. S., Kunitomo, M., & Takahashi, S. Z. 2016, MNRAS, 461, 2257, doi: 10.1093/mnras/stw1531

Kirchschlager, F., Bertrang, G. H. M., & Flock, M. 2019, MNRAS, 488, 1211, doi: 10.1093/mnras/stz1763

Kirk, J. M., Ward-Thompson, D., & André, P. 2005, MNRAS, 360, 1506, doi: 10.1111/j.1365-2966.2005.09145.x

Komaki, A., Nakatani, R., & Yoshida, N. 2021, ApJ, 910, 51, doi: 10.3847/1538-4357/abe2af

Kroupa, P. 2001, MNRAS, 322, 231, doi: 10.1046/j.1365-8711.2001.04022.x

Labdon, A., Kraus, S., Davies, C. L., et al. 2021, A&A, 646, A102, doi: 10.1051/0004-6361/202039370

Lada, C. J. 1987, in Star Forming Regions, ed. M. Peimbert & J. Jugaku, Vol. 115, 1

Lambrechts, M., & Johansen, A. 2012, A&A, 544, A32, doi: 10.1051/0004-6361/201219127

—. 2014, A&A, 572, A107, doi: 10.1051/0004-6361/201424343

Lambrechts, M., Morbidelli, A., Jacobson, S. A., et al. 2019, A&A, 627, A83, doi: 10.1051/0004-6361/201834229

Lee, Y.-N., Charnoz, S., & Hennebelle, P. 2021, A&A, 648, A101, doi: 10.1051/0004-6361/202038105

Liu, B., Lambrechts, M., Johansen, A., & Liu, F. 2019, A&A, 632, A7, doi: 10.1051/0004-6361/201936309

Liu, Y., Linz, H., Fang, M., et al. 2022, A&A, 668, A175, doi: 10.1051/0004-6361/202244505

Lynden-Bell, D., & Pringle, J. E. 1974, MNRAS, 168, 603, doi: 10.1093/mnras/168.3.603

Macías, E., Guerra-Alvarado, O., Carrasco-González, C., et al. 2021, A&A, 648, A33, doi: 10.1051/0004-6361/202039812

Mamajek, E. E. 2009, in American Institute of Physics Conference Series, Vol. 1158, Exoplanets and Disks: Their Formation and Diversity, ed. T. Usuda, M. Tamura, & M. Ishii, 3–10, doi: 10.1063/1.3215910

Manara, C. F., Ansdell, M., Rosotti, G. P., et al. 2023, in Astronomical Society of the Pacific Conference Series, Vol. 534, Protostars and Planets VII, ed. S. Inutsuka, Y. Aikawa, T. Muto, K. Tomida, & M. Tamura, 539, doi: 10.48550/arXiv.2203.09930

Manara, C. F., Rosotti, G., Testi, L., et al. 2016, A&A, 591, L3, doi: 10.1051/0004-6361/201628549

Manara, C. F., Testi, L., Herczeg, G. J., et al. 2017, A&A, 604, A127, doi: 10.1051/0004-6361/201630147

Mayor, M., & Queloz, D. 1995, Nature, 378, 355, doi: 10.1038/378355a0

McKee, C. F., & Ostriker, E. C. 2007, ARA&A, 45, 565, doi: 10.1146/annurev.astro.45.051806.110602

Menou, K., & Goodman, J. 2004, ApJ, 606, 520, doi: 10.1086/382947

Michel, A., Sadavoy, S. I., Sheehan, P. D., et al. 2023, AJ, 166, 184, doi: 10.3847/1538-3881/acf653

Michel, A., van der Marel, N., & Matthews, B. C. 2021, ApJ, 921, 72, doi: 10.3847/1538-4357/ac1bbb

Miotello, A., Kamp, I., Birnstiel, T., Cleeves, L. C., & Kataoka, A. 2023, in Astronomical Society of the Pacific Conference Series, Vol. 534, Protostars and Planets VII, ed. S. Inutsuka, Y. Aikawa, T. Muto, K. Tomida, & M. Tamura, 501, doi: 10.48550/arXiv.2203.09818

Mohanty, S., Jayawardhana, R., & Basri, G. 2005, ApJ, 626, 498, doi: 10.1086/429794

Musiolik, G., Teiser, J., Jankowski, T., & Wurm, G. 2016a, ApJ, 818, 16, doi: 10.3847/0004-637X/818/1/16

—. 2016b, ApJ, 827, 63, doi: 10.3847/0004-637X/827/1/63

Muzerolle, J., Hillenbrand, L., Calvet, N., Briceño, C., & Hartmann, L. 2003, ApJ, 592, 266, doi: 10.1086/375704

Nakagawa, Y., Sekiya, M., & Hayashi, C. 1986, Icarus, 67, 375, doi: 10.1016/0019-1035(86)90121-1

Natta, A., Testi, L., Calvet, N., et al. 2007, in Protostars and Planets V, ed. B. Reipurth, D. Jewitt, & K. Keil, 767, doi: 10.48550/arXiv.astro-ph/0602041

Natta, A., Testi, L., & Randich, S. 2006, A&A, 452, 245, doi: 10.1051/0004-6361:20054706

Nielbock, M., Launhardt, R., Steinacker, J., et al. 2012, A&A, 547, A11, doi: 10.1051/0004-6361/201219139

Ohashi, N., Tobin, J. J., Jørgensen, J. K., et al. 2023, ApJ, 951, 8, doi: 10.3847/1538-4357/acd384

Ormel, C. W., & Klahr, H. H. 2010, A&A, 520, A43, doi: 10.1051/0004-6361/201014903

Ormel, C. W., Liu, B., & Schoonenberg, D. 2017, A&A, 604, A1, doi: 10.1051/0004-6361/201730826

Ormel, C. W., Paszun, D., Dominik, C., & Tielens, A. G. G. M. 2009, A&A, 502, 845, doi: 10.1051/0004-6361/200811158

Panahi, A., Zucker, S., Clementini, G., et al. 2022, A&A, 663, A101, doi: 10.1051/0004-6361/202243497

Pascucci, I., Cabrit, S., Edwards, S., et al. 2023, in Astronomical Society of the Pacific Conference Series, Vol. 534, Protostars and Planets VII, ed. S. Inutsuka, Y. Aikawa, T. Muto, K. Tomida, & M. Tamura, 567, doi: 10.48550/arXiv.2203.10068

Pascucci, I., Testi, L., Herczeg, G. J., et al. 2016, ApJ, 831, 125, doi: 10.3847/0004-637X/831/2/125

Perryman, M., Hartman, J., Bakos, G. Á., & Lindegren, L. 2014, ApJ, 797, 14, doi: 10.1088/0004-637X/797/1/14

Pfalzner, S., Steinhausen, M., & Menten, K. 2014, ApJL, 793, L34, doi: 10.1088/2041-8205/793/2/L34

Picogna, G., Ercolano, B., & Espaillat, C. C. 2021, MNRAS, 508, 3611, doi: 10.1093/mnras/stab2883

Pineda, J. E., Arzoumanian, D., Andre, P., et al. 2023, in Astronomical Society of the Pacific Conference Series, Vol. 534, Protostars and Planets VII, ed. S. Inutsuka, Y. Aikawa, T. Muto, K. Tomida, & M. Tamura, 233, doi: 10.48550/arXiv.2205.03935

Pinilla, P., Pascucci, I., & Marino, S. 2020, A&A, 635, A105, doi: 10.1051/0004-6361/201937003

Pinilla, P., Pohl, A., Stammler, S. M., & Birnstiel, T. 2017, ApJ, 845, 68, doi: 10.3847/1538-4357/aa7edb

Pollack, J. B., Hollenbach, D., Beckwith, S., et al. 1994, ApJ, 421, 615, doi: 10.1086/173677

Pollack, J. B., Hubickyj, O., Bodenheimer, P., et al. 1996, Icarus, 124, 62, doi: 10.1006/icar.1996.0190

Pringle, J. E. 1981, ARA&A, 19, 137, doi: 10.1146/annurev.aa.19.090181.001033

Ribas, Á., Bouy, H., & Merín, B. 2015, A&A, 576, A52, doi: 10.1051/0004-6361/201424846

Ribas, Á., Espaillat, C. C., Macías, E., & Sarro, L. M. 2020, A&A, 642, A171, doi: 10.1051/0004-6361/202038352

Ribas, Á., Merín, B., Bouy, H., & Maud, L. T. 2014, A&A, 561, A54, doi: 10.1051/0004-6361/201322597

Ricci, L., Testi, L., Natta, A., et al. 2010, A&A, 512, A15, doi: 10.1051/0004-6361/200913403

Ricci, L., Trotta, F., Testi, L., et al. 2012, A&A, 540, A6, doi: 10.1051/0004-6361/201118296

Ruíz-Rodríguez, D., Cieza, L. A., Williams, J. P., et al. 2018, MNRAS, 478, 3674, doi: 10.1093/mnras/sty1351

Sanchis, E., Testi, L., Natta, A., et al. 2020, A&A, 633, A114, doi: 10.1051/0004-6361/201936913

Sellek, A. D., Clarke, C. J., & Ercolano, B. 2022, MNRAS, 514, 535, doi: 10.1093/mnras/stac1148

Shakura, N. I., & Sunyaev, R. A. 1973, A&A, 24, 337

Shu, F. H. 1977, ApJ, 214, 488, doi: 10.1086/155274

Sozzetti, A., Giacobbe, P., Lattanzi, M. G., et al. 2014, MNRAS, 437, 497, doi: 10.1093/mnras/stt1899

Stammler, S. M., Lichtenberg, T., Drążkowska, J., & Birnstiel, T. 2023, A&A, 670, L5, doi: 10.1051/0004-6361/202245512

Suzuki, T. K., Ogihara, M., Morbidelli, A., Crida, A., & Guillot, T. 2016, A&A, 596, A74, doi: 10.1051/0004-6361/201628955

Tabone, B., Rosotti, G. P., Cridland, A. J., Armitage, P. J., & Lodato, G. 2022a, MNRAS, 512, 2290, doi: 10.1093/mnras/stab3442

Tabone, B., Rosotti, G. P., Lodato, G., et al. 2022b, MNRAS, 512, L74, doi: 10.1093/mnrasl/slab124

Takahashi, S. Z., Inutsuka, S.-i., & Machida, M. N. 2013, ApJ, 770, 71, doi: 10.1088/0004-637X/770/1/71

Takakuwa, S., Saigo, K., Kido, M., et al. 2024, arXiv e-prints, arXiv:2401.08722, doi: 10.48550/arXiv.2401.08722

Tazzari, M., Clarke, C. J., Testi, L., et al. 2021a, MNRAS, 506, 2804, doi: 10.1093/mnras/stab1808

Tazzari, M., Testi, L., Natta, A., et al. 2021b, MNRAS, 506, 5117, doi: 10.1093/mnras/stab1912

Teague, R., Hull, C. L. H., Guilloteau, S., et al. 2021, ApJ, 922, 139, doi: 10.3847/1538-4357/ac2503

Teixeira, P. S., Lada, C. J., & Alves, J. F. 2005, ApJ, 629, 276, doi: 10.1086/430849

Tobin, J. J., Looney, L. W., Li, Z.-Y., et al. 2018, ApJ, 867, 43, doi: 10.3847/1538-4357/aae1f7

Trapman, L., Facchini, S., Hogerheijde, M. R., van Dishoeck, E. F., & Bruderer, S. 2019, A&A, 629, A79, doi: 10.1051/0004-6361/201834723

Trapman, L., Miotello, A., Kama, M., van Dishoeck, E. F., & Bruderer, S. 2017, A&A, 605, A69, doi: 10.1051/0004-6361/201630308

Tripathi, A., Andrews, S. M., Birnstiel, T., & Wilner, D. J. 2017, ApJ, 845, 44, doi: 10.3847/1538-4357/aa7c62

Tychoniec, Ł., Tobin, J. J., Karska, A., et al. 2018, ApJS, 238, 19, doi: 10.3847/1538-4365/aaceae

Tychoniec, Ł., Manara, C. F., Rosotti, G. P., et al. 2020, A&A, 640, A19, doi: 10.1051/0004-6361/202037851

Ueda, T., Kataoka, A., Zhang, S., et al. 2021, ApJ, 913, 117, doi: 10.3847/1538-4357/abf7b8

van der Marel, N., & Mulders, G. D. 2021, AJ, 162, 28, doi: 10.3847/1538-3881/ac0255

Villenave, M., Ménard, F., Dent, W. R. F., et al. 2021, A&A, 653, A46, doi: 10.1051/0004-6361/202140496

Vlemmings, W. H. T., Lankhaar, B., Cazzoletti, P., et al. 2019, A&A, 624, L7, doi: 10.1051/0004-6361/201935459

Weidenschilling, S. J. 1977, MNRAS, 180, 57, doi: 10.1093/mnras/180.1.57

Williams, J. P., Cieza, L., Hales, A., et al. 2019, ApJL, 875, L9, doi: 10.3847/2041-8213/ab1338

Winter, A. J., & Haworth, T. J. 2022, European Physical Journal Plus, 137, 1132, doi: 10.1140/epjp/s13360-022-03314-1

Woitke, P., Min, M., Pinte, C., et al. 2016, A&A, 586, A103, doi: 10.1051/0004-6361/201526538

Wurster, J., Bate, M. R., & Price, D. J. 2019, MNRAS, 489, 1719, doi: 10.1093/mnras/stz2215

Yang, H., & Bai, X.-N. 2021, ApJ, 922, 201, doi: 10.3847/1538-4357/ac250a

Zhang, S., Kalscheur, M., Long, F., et al. 2023, ApJ, 952, 108, doi: 10.3847/1538-4357/acd334

Zhu, W., Petrovich, C., Wu, Y., Dong, S., & Xie, J. 2018, ApJ, 860, 101, doi: 10.3847/1538-4357/aac6d5

Zhu, Z., Hartmann, L., & Gammie, C. 2009, ApJ, 694, 1045, doi: 10.1088/0004-637X/694/2/1045

Part II

Scientific Publications

Author contributions

My contributions to each paper is presented here.

Paper I

Dust clearing by radial drift in protoplanetary discs
J. Appelgren, M. Lambrechts, and A. Johansen (2020)

The original idea for this project was proposed by Michiel Lambrechts (ML). I developed the model and wrote the code, with contributions from ML, used to perform the simulations. I led the analysis of the simulations and the writing of the article, with comments from Anders Johansen (AJ) and ML.

Paper II

Disc population synthesis: decrease of the solid mass reservoir through pebble drift
J. Appelgren, M. Lambrechts, N. van der Marel (2023)

I built upon the model used in paper I and wrote the code to implement the updates, including a complete rewrite of the code to a more optimized and user friendly state. I ran the simulations and led the analysis of them. I led the writing of the article with comments from ML and Nienke van der Marel (NM).

Paper III

The evolution of the flux-size relationship in protoplanetary discs by viscous evolution and radial pebble drift
J. Appelgren, A. Johansen, M. Lambrechts, J. Jørgensen, and N. van der Marel (to be submitted)

I used the model developed for paper II to run the simulations that are the basis of the results of the paper. I led the analysis of the simulations and led the writing of the article with comments from the co-authors.